FAZST-Femto-Atto-ZeptoSecond Science & Technology

Andre D Bandrauk,FRSC,FAAAS
Canada Research Chair
Computational Chemistry&Molecular Photonics
Universite de Sherbrooke
http://pages.usherbrooke.ca/adbandrauk

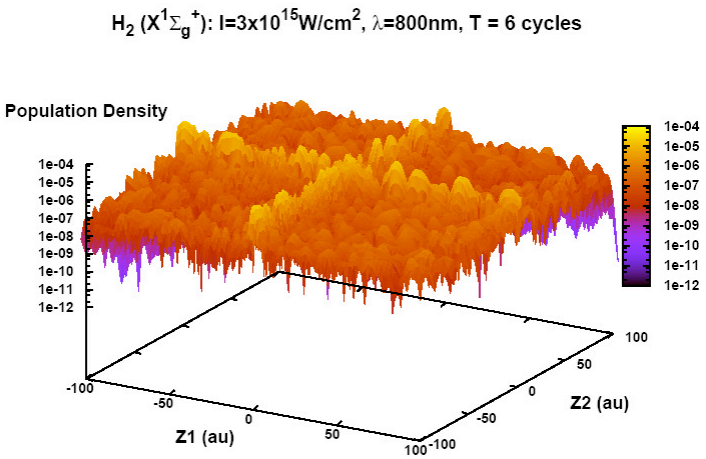

“Molecules in Intense Laser Fields – Femto to Atto to ZeptoSecond Dynamics”

and / or

“FAZSST-Femto-Atto-ZeptoSecond Science & Technology”

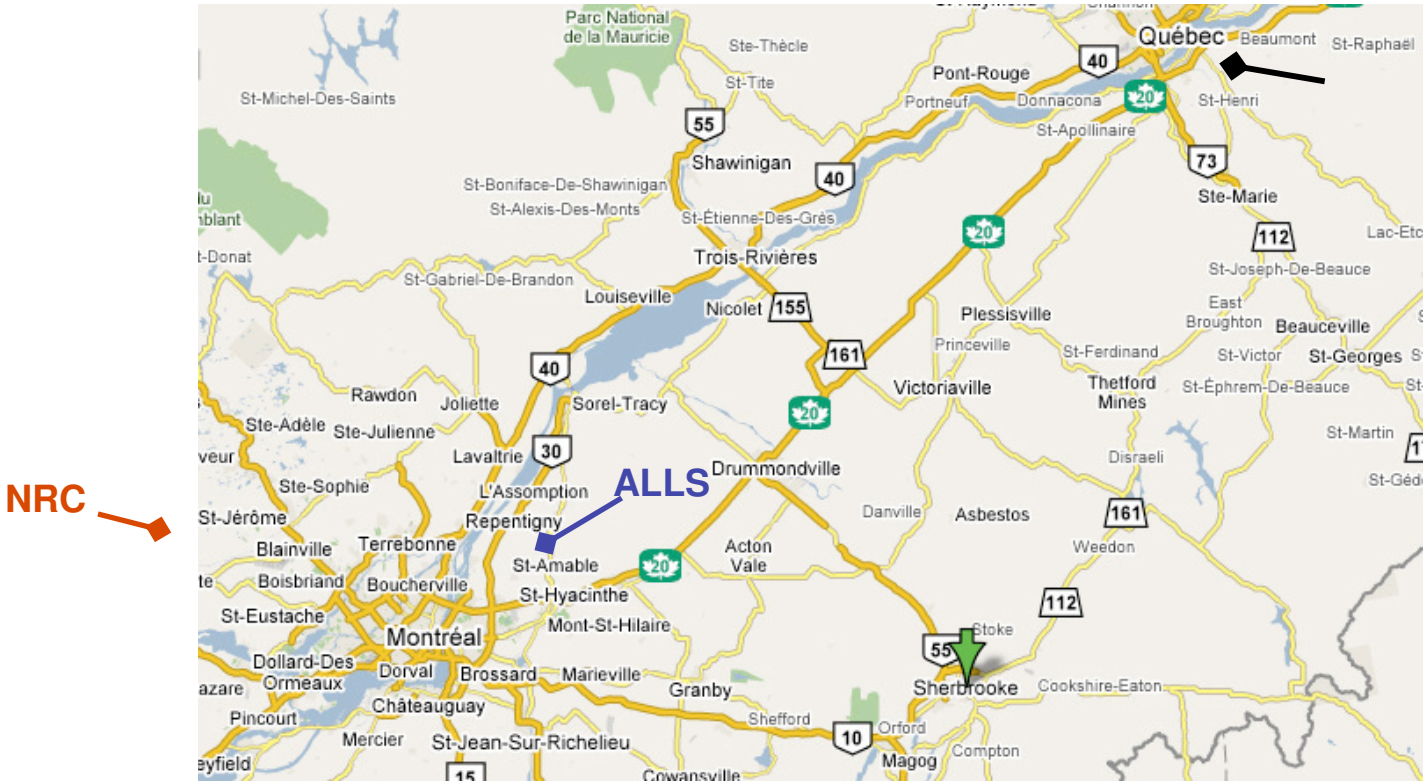

André D, Bandrauk, PhD, FRSC, FAAAS
Canada Research Chair
Computational Chemistry & Molecular Photonics
Université de Sherbrooke

Potential energy : $V_o : \frac{e^2}{a_0} = 1\ Hartree = 27.2\ eV,$ (1)

Electric field $E_o : \frac{e}{a_o^2} = 5 \times 10^9\ V/cm,$ (2)

Intensity $I_0 = cE_0^2/8\pi = 3.5 \times 10^{16}\ W/cm^2,$ (3)

Distance $a_0 = 0.0529 nm,$ (4)

Time : $t(a_0)$=24 as, $2\pi t_0$=152 as
$t(mc^2)$=1.3 zeptos

Table I

Evolution of Laser Parameters [1]

Time (s)		Intensity (Watts/cm²)		Year
Nano	10^{-9}	Giga	10^{+9}	1980
Pico	10^{-12}	Tera	10^{+12}	1985
SERS				
Femto	10^{-15}	Peta	10^{+15}	1990
1a.u : 24 x 10^{-18}		$I_0 = 3.5 \times 10^{+16}$		
Atto	10^{-18}	Exa	10^{+18}	2005
Zepto	10^{-21}	Zetta	10^{+21}	2009
Yocto	10^{-24}	Yotta	10^{+24}	?

10^{29} - **Schwinger Limit**

The intensities discussed in the present article, $10^{14} \geq I \geq 10^{15} W/cm^2$ correspond to fields approaching the internal Coulomb potentials of atoms and molecules (V_0, equations (1-3), thus inducing considerable distortions of intermolecular potentials. In the dressed state representation these radiatively induced distortions creating LIMP's as discussed above lead to *bond softening* via laser-induced avoided crossing of molecular potentials [26-27]. At such intensities, one needs to consider further ionization and the remaining molecular ion potentials become LIMP's in the presence of intense laser pulses. The molecular ions, bound or dissociative can also undergo Above Threshold Dissociation, ATD, [20], [26-27],

Schwinger limit ~ 10**29 W/cm2)

Sunlight: 0.12 W/cm2

F Krausz,MPQ,MUenchen

structure and dynamics in the microcosm

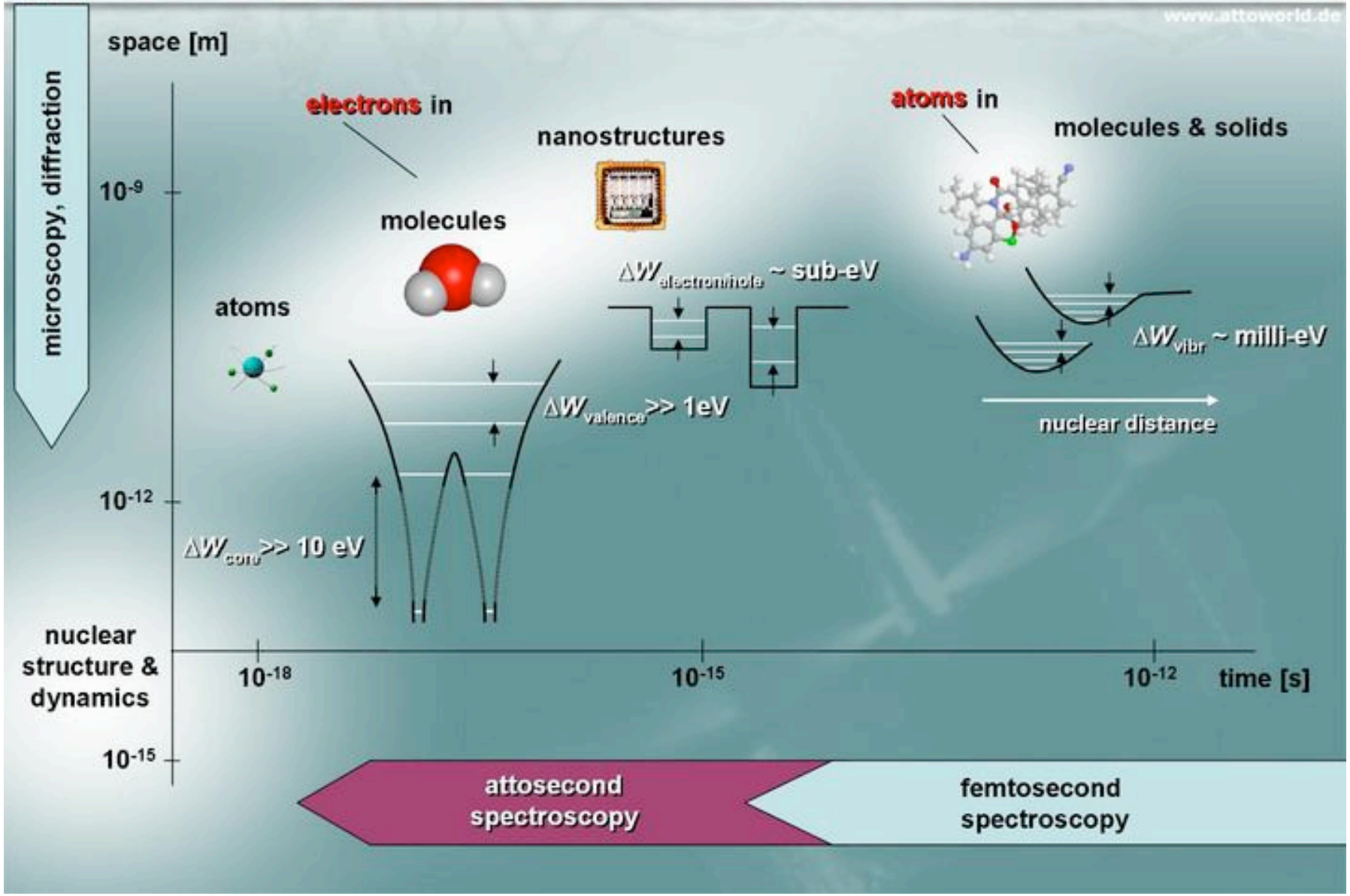

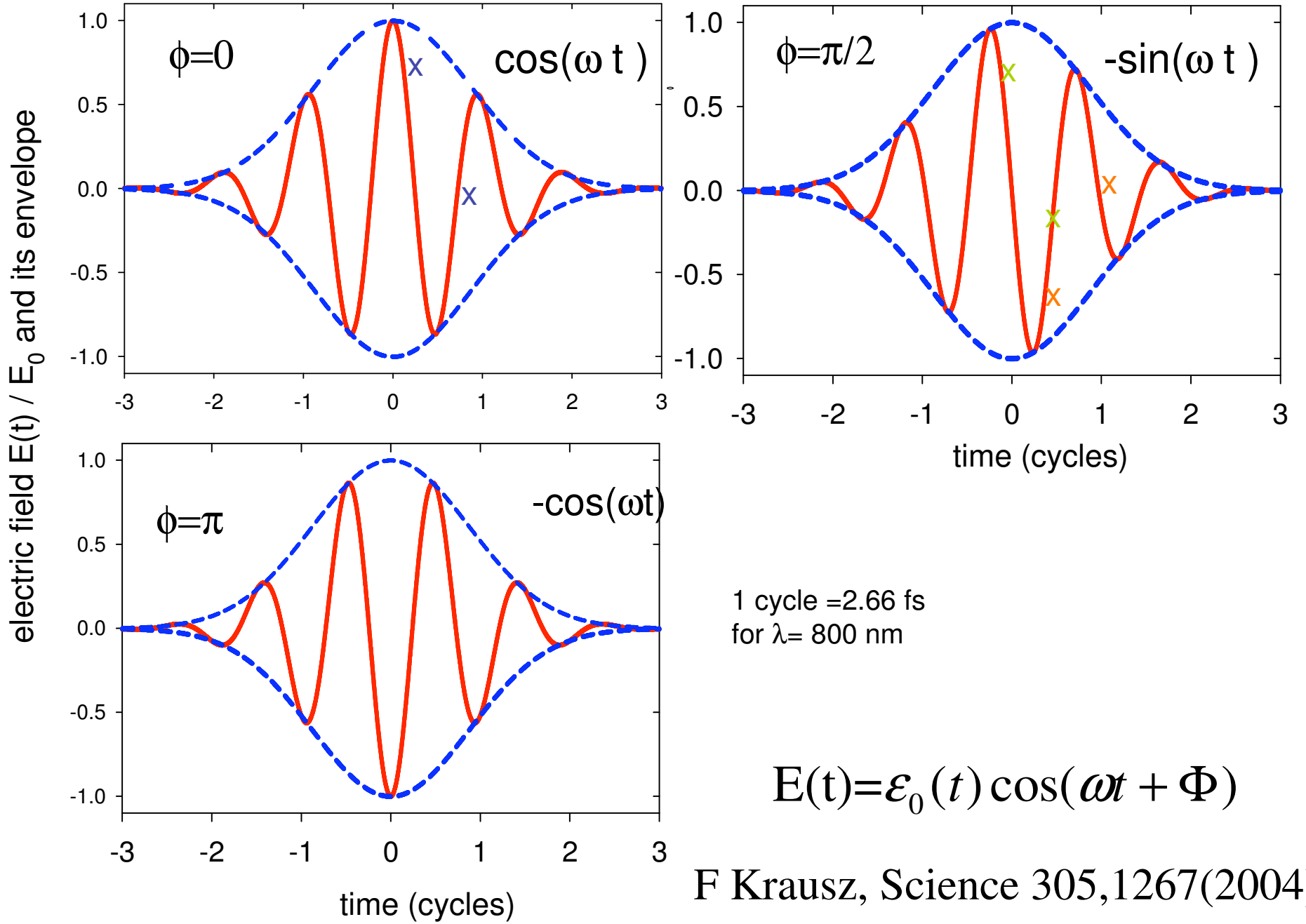

1 cycle =2.66 fs
for λ= 800 nm

$$E(t)=\varepsilon_0(t)\cos(\omega t+\Phi)$$

F Krausz, Science 305,1267(2004)

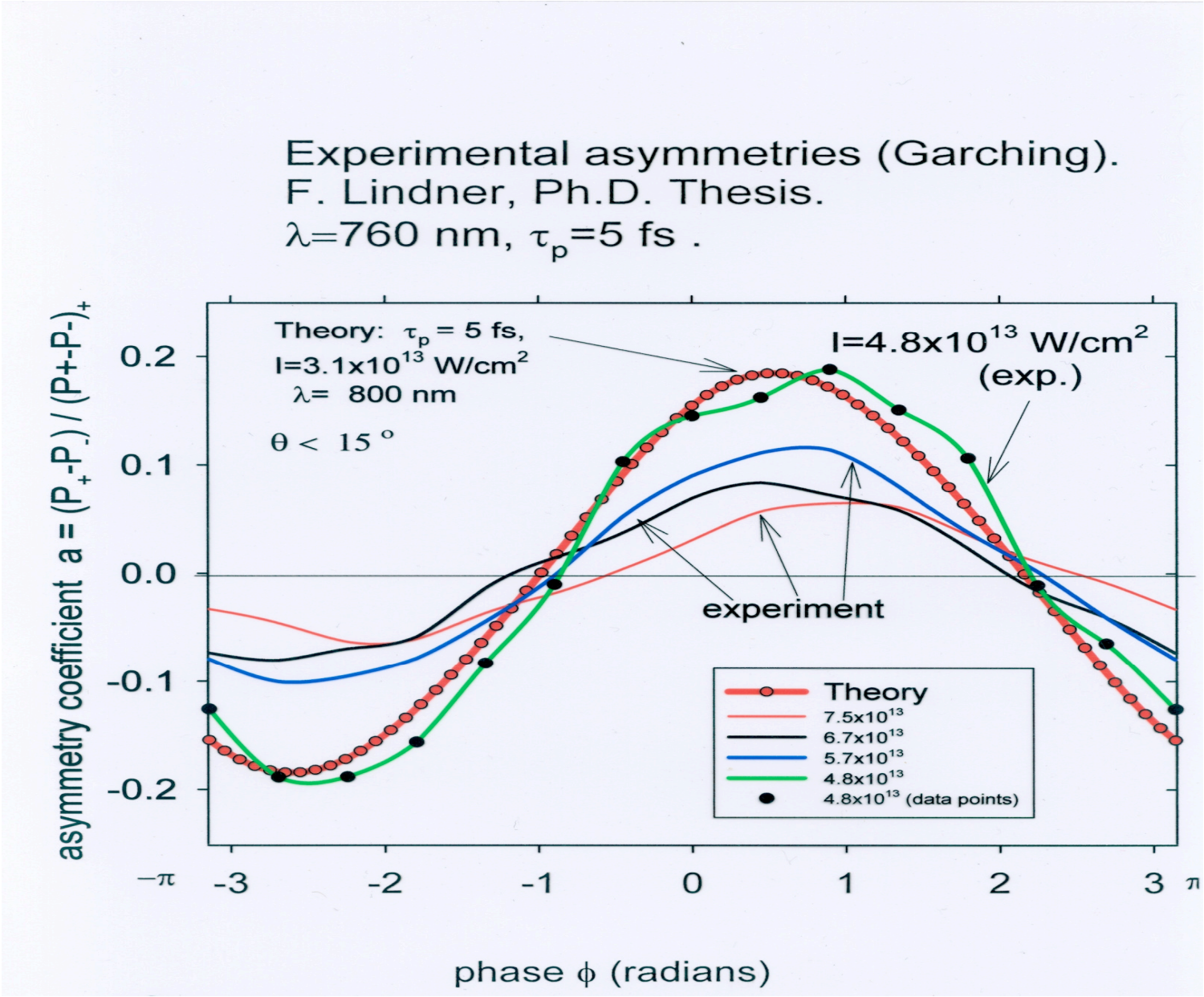

- **Phys. Rev. A, 70, 013815 (2004)**
- **Opt. Lett. 29, 1557 (2004)**

Science

Exciting electrons

Chemistry rarely grabs the limelight. But in 2011 it will try to

Nov 22nd 2010 | from PRINT EDITION

One sugar, please

Les lasers traquent les mouvements des électrons

>>> *Science* en juin, par une équipe internationale conduite par Martin Schultze, de l'université Ludwig Maximilians et du Max Planck Institut d'optique quantique, à Garching. Ils ont observé, pour la première fois, un délai entre les différents processus d'émissions de lumière provoqués par l'excitation d'un atome de néon. Un délai de 21 attosecondes, mesuré à 5 attosecondes près [8]. *« On observe là un phénomène que personne ne peut encore expliquer,* insiste Anne L'Huillier, *c'est vraiment de la nouvelle physique. »*

Manipulation à volonté. Tout aussi enthousiaste, Eleftherios Goulielmakis décrit déjà les prochaines étapes : *« Après les premières études sur des atomes simples, la physique attoseconde se tourne vers l'étude de molécules de plus en plus complexes, de plus en plus grosses. Progressivement, les efforts se porteront sur les macromolécules, par exemple les peptides pour la biochimie, ou les molécules mises en jeu dans le processus de la photosynthèse, et enfin pour progresser en physique des solides. »*

Pour le physicien, l'étape suivante sera alors de manipuler les électrons à l'aide des impulsions attosecondes : *« Nous travaillons à mettre au point une boîte à outils en ce sens, par exemple en sculptant la forme des impulsions pour agir sur les électrons. »* De quoi placer la physique attoseconde sur la voie dessinée, depuis les années 1980, par la microscopie à effet tunnel et à force atomique*. D'instruments imaginés au départ pour épier la matière ces microscopes ont fini par devenir de véritables couteaux suisses, permettant de manipuler atomes et molécules à volonté, à l'échelle du nanomètre. Les impulsions attosecondes en feront-elles autant avec des électrons, permettant par exemple de contrôler l'efficacité de certaines réactions chimiques, comme la photosynthèse ? *« Nous verrons les premiers résultats d'outils attosecondes dès l'an prochain »*, pronostique Eleftherios Goulielmakis.

*** LE MICROSCOPE À EFFET TUNNEL** utilise un phénomène quantique, l'effet tunnel, pour déterminer la topologie de surfaces avec une résolution voisine du nanomètre. Le microscope à force atomique en est un dérivé.

Attophysique. À quand aussi une « attoélectronique » capable de redonner un coup de fouet à la physique des semi-conducteurs qui s'approche de ses limites ? Pour Anne L'Huillier, on en est encore loin : *« Tout le monde y pense bien évidemment mais rien n'est encore fait. Comme nous défrichons un domaine complètement vierge, de nouvelles questions surgissent à chaque résultat expérimental. C'est pour cette raison que le délai entre les expériences et les publications est très long. Il nous faut le temps de comprendre ce qu'on observe. »* De longs mois d'interprétation qui n'empêchent pas la véritable moisson de publications constatée cette année, et qui augurent déjà une année 2011 au moins aussi riche. Et notamment en Europe, puisque les réseaux de coopération scientifique sur la physique attoseconde qui s'y succèdent depuis 1992 – le dernier en date, Attofel, vient de démarrer – ont permis au Vieux Continent de prendre la tête de la compétition internationale pour la maîtrise de cette nouvelle physique. ■

Une moisson de prix

Signe du fort dynamisme de la discipline, la physique attoseconde a eu les honneurs de trois prix prestigieux l'automne dernier. Anne L'Huillier (photo), de l'université de Lund, en Suède, est l'une des cinq lauréates du prix 2011 « Pour les femmes et la science » remis par l'Unesco et la fondation L'Oréal. Le jury était présidé cette année par le Prix Nobel Ahmed Zewail, couronné en 1999 pour ses travaux en physique femtoseconde. Début novembre, André Bandrauk, de l'université de Sherbrooke, au Canada, a reçu le prix Marie-Victorin, l'un des onze Prix du Québec remis chaque année par le gouvernement de la province canadienne. André Bandrauk est un théoricien qui a notamment travaillé sur le comportement des molécules dans des champs électromagnétiques intenses et la génération d'harmoniques. Enfin, mi-novembre, l'Autrichien Reihnard Kienberger s'est vu remettre le prix annuel de la Commission internationale pour l'optique (ICO). Il travaille en particulier sur la mesure des impulsions attosecondes uniques, au Max Planck Institut d'optique quantique, à Garching, en Allemagne. Tout comme Eleftherios Goulielmakis, récompensé cette année par le Prix du jeune chercheur de l'ICO. Si tout le monde se refuse à l'évoquer, l'idée qu'un Nobel puisse récompenser un jour l'« attophysique » est présente dans toutes les têtes.

[1] Pascal Salières, Thierry Ruchon et Bertand Carré, « Des flashs toujours plus courts », *Les Dossiers de la Recherche*, p. 60, février 2010 ; Timothée Jamin, « Filmer le mouvement des électrons », *La Recherche*, novembre 2010, p. 68.
[2] D. H. Ko *et al.*, *New J. Phys.*, doi : 12063008, 2010.
[3] S. Haessler *et al.*, *Nature Physics*, 6, 200, 2010.
[4] E. Goulielmakis *et al.*, *Nature*, 466, 739, 2010.
[5] G. Sansone *et al.*, *Nature*, 465, 763, 2010.
[6] Y. Mairesse *et al.*, *Phys. Rev. Lett.*, 104, doi : 213601, 2010.
[7] H. Wörner *et al.*, *Nature*, 466, 604, 2010.
[8] M. Schultze *et al.*, *Science*, 328, 1658, 2010.

MAXWELL – SCHROEDINGER

Classical **Quantum**

MAXWELL

$$\boxed{\frac{\partial^2 E}{\partial z^2} - \frac{1}{c^2}\frac{\partial^2 E}{\partial t^2} = \frac{4\pi}{c^2}\frac{\partial^2 P}{\partial t^2}}$$

P = Medium Polarization = P(E)

(1st Order P = αE)

SCHROEDINGER

$$\boxed{i\hbar\frac{\partial|\psi\rangle}{\partial t} = \left(\hat{H}_0 + \hat{V}(t)\right)|\psi\rangle}$$

$$P = P(E) = n_0\langle\psi|\hat{\mu}_0|\psi\rangle$$

$$|\psi\rangle = \sum_j c_j e^{iE_j t/\hbar}|\Psi_j\rangle$$

$$V_{ii} = -P_{ii}\left(e(z,t)\cos(kz-\omega t)\right)$$

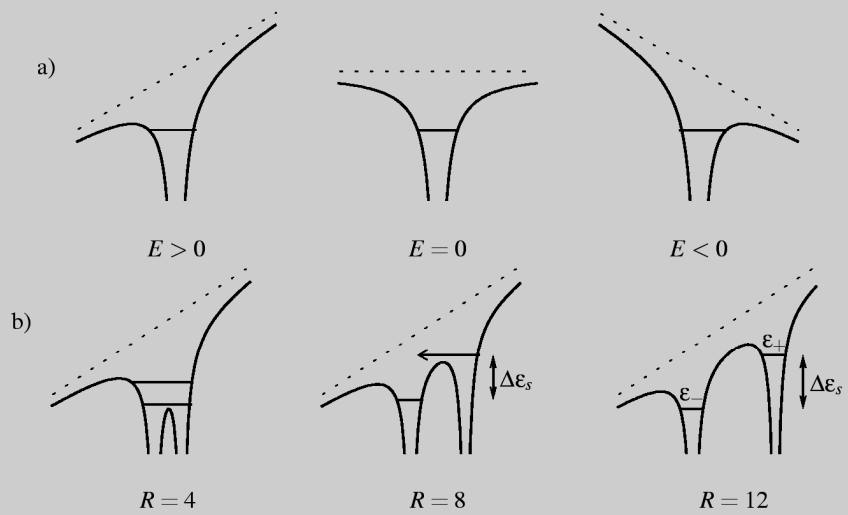

Figure 1. (a) Atomic electronic potentials distorted respectively by the presence of a strong positive, null, and negative external electric field. (b) Electronic molecular ptoentials in a positive electric field, as a function of the internuclear distance R. The Stark shift $\Delta\epsilon_S$ between the two localized molecular orbitals ϵ_+ and $\epsilon_- \simeq E_{max}R$.

P. B. Corkum, PRL, 71, 1994 (1993).

T. Zuo and A. D. Bandrauk, PRA, 52, R2511 (1995).

feature article

Recollision physics

Paul B. Corkum

A technique that uses light to create particle collisions that create light is poised to provide unprecedented access to the inner workings of atoms and molecules.

Paul Corkum is a professor of physics at the University of Ottawa and director of attosecond science at the National Research Council Canada, both in Ontario.

In 1906 Ernest Rutherford discovered that α particles deflect as they pass through a mica film. That experiment, which helped Rutherford identify the atomic nucleus, was a dramatic demonstration that collisions between particles could tell us about the structure of matter. Now, a century later, high-energy collisions between subatomic particles have revealed the fundamental building blocks of our world—quarks, muons, and so on—and lower-energy collisions have been central to understanding and harnessing nuclear physics.

Just over 50 years after Rutherford's experiment, the laser was demonstrated. Since then, optical physics, which deals with interactions between light and matter, has developed powerful methods for exciting, probing, and controlling matter and its dynamics. The precision of optical experiments has reached the point where some of the most fundamental questions of particle physics can be tested better optically than by collisions.

Although optical and collision physics are traditionally considered separate disciplines sharing little, if any, overlap, the emerging field of recollision physics unites the two. In a recollision, the oscillating field of a laser pulse causes an electron to accelerate away from an atom or molecule and then, upon reversal of the field, careen back into its parent ion. Whereas traditional collision physics relies on large accelerators and magnets to arrange the collision, in recollision physics it is the laser field that provides the acceleration and the atom itself that provides the electron with which it is probed. Through recollision, optics gains access to the well-developed capability to probe the structure of matter via collisions (the focus of this article) and collision physics gains access to the capability to excite, probe, and control matter with light.

Two coherence transfers

Consider an atom illuminated by a pulse of coherent IR light. If the light is intense enough, roughly 10^{13} W/cm^2 or higher (see box 1), then at each crest of the oscillating electromagnetic field, the valence-electron wavefunction will partially ionize, so-called tunnel ionization. Strictly speaking, tunneling is a DC phenomenon. However, Leonid Keldysh showed nearly half a century ago that multiphoton ionization can approximate tunneling in atoms and solids when IR light is used.[1] Thus, I will speak of laser tunneling, or simply tunneling, throughout the paper. Through tunneling, the coherent light pulse splits the electron wavefunction into two mutually coherent parts—the bound-state wavefunction and the tunnel-ionized wavepacket. (See figure 1.)

Once the electron has tunneled, the resulting wavepacket—now in the continuum, freed from the pull of its parent ion—is driven in a semiclassical motion by the laser field. The classical approximation of subcycle electron motion has a long history in plasma physics.[2] It is useful when many photons are involved.

What happens next depends on the polarization of the light pulse. If the polarization is circular, then as soon as any portion of the wavepacket emerges from the atom or mole-

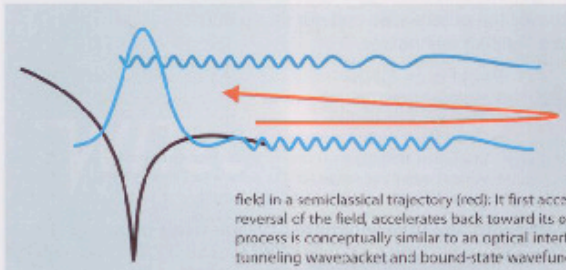

Figure 1. The basics of recollision. In the first step, an intense pulse of coherent IR light skews the potential well (black) of an atom or molecule's electron. That allows the bound-state electron wavefunction (blue, sketched as a Gaussian) to tunnel and split, creating a wavepacket in the continuum. There, the wavepacket is driven by the oscillating laser field in a semiclassical trajectory (red): It first accelerates away from the atom and then, upon reversal of the field, accelerates back toward its origin, recolliding with its parent ion. The process is conceptually similar to an optical interferometer. The relative wavelengths of the tunneling wavepacket and bound-state wavefunction are illustrated approximately to scale.

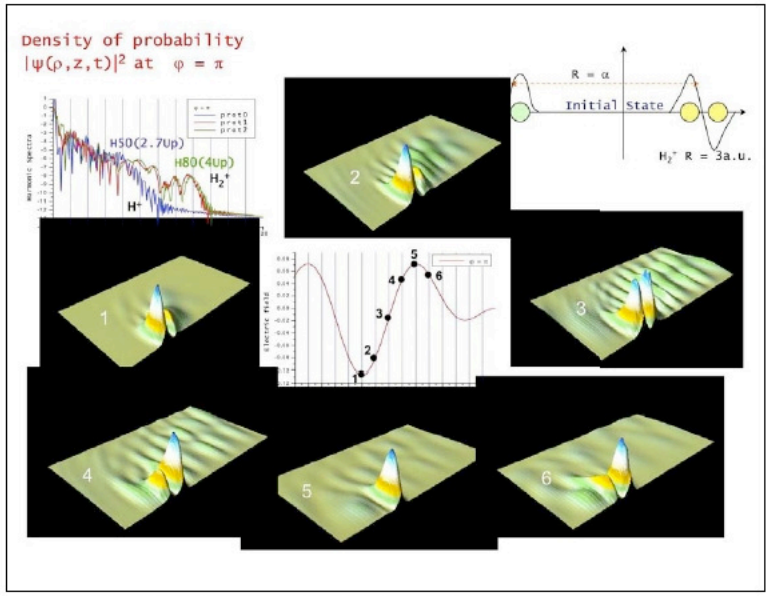

Le sytème moléculaire H^+ (gauche) + H_2^+ (droite) en présence d'un champ (électrique) laser

On voit la distribution ondulatoire de l'électron se déplacer de gauche à droite selon l'intensité du champ (dont les valeurs sont données par les points de 1 à 6). Une partie de l'électron se dissipe comme des ondes d'eau à cause de l'ionisation.

ADB,S.Barmaki,GKamta

PhysRevLett 98,013001 (2007)

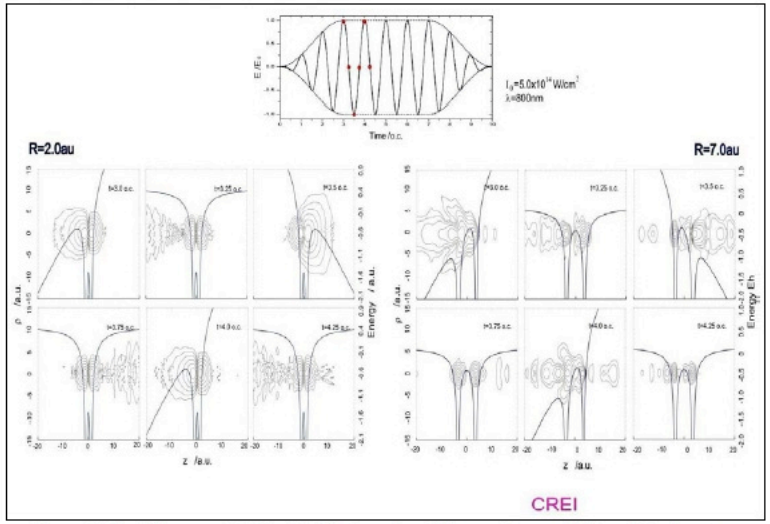

Exemple de déplacement de l'onde d'électron dans H_2^+ en présence de l'impulsion laser (à des distances internucléaires différentes)

On voit l'électron suivre plus ou moins le champ électrique (représenté par un point rouge), ce qui permet d'envisager le contrôle du mouvement d'un électron dans une molécule par laser en dépit de la nature ondulatoire de l'électron.

KJ Yuan,ADB
PRA 80,053404 (2009)

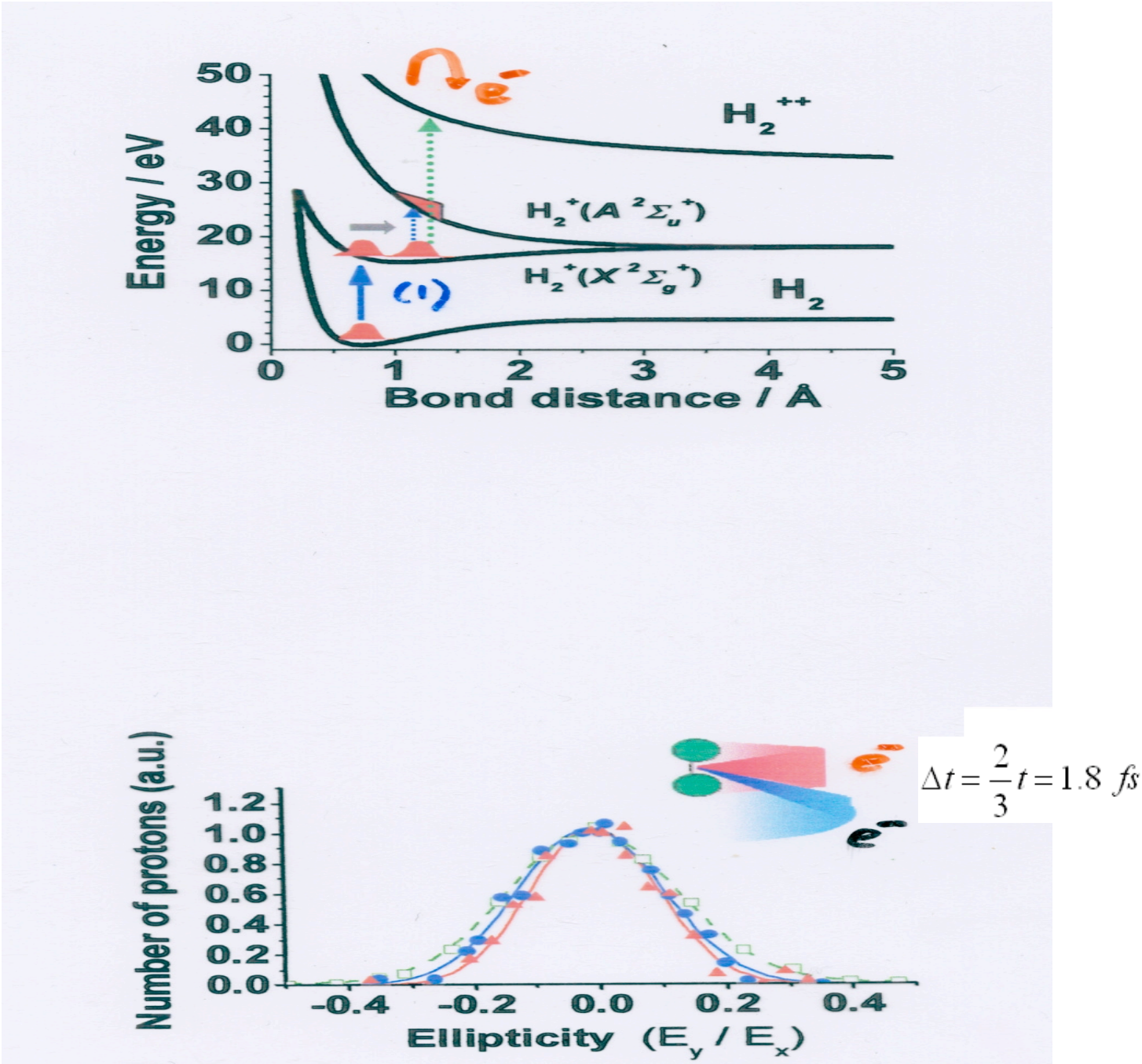

Nature 417, p. 917 (2002)

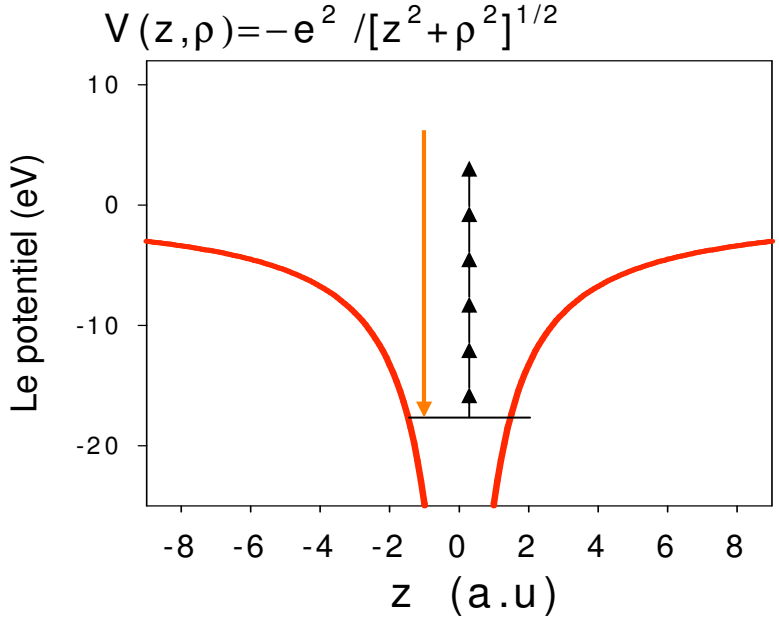

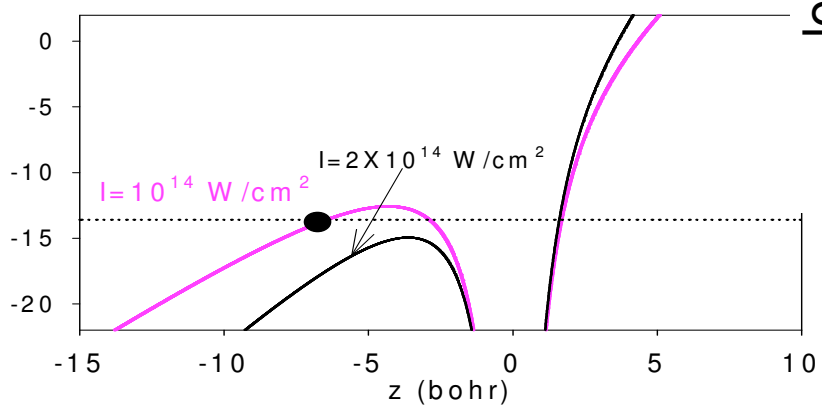

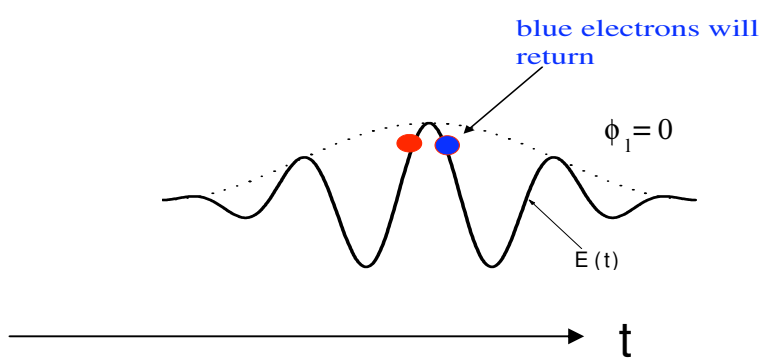

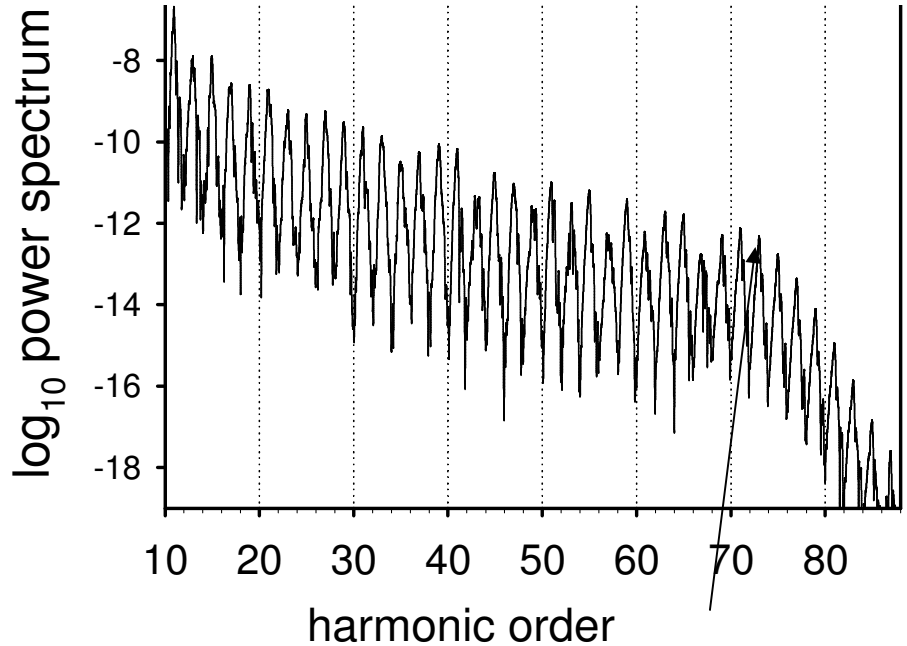

Cuttof at:

$$n_{cut} = [I_p + 3.17\ U_p]/\omega_L\ , \quad \mathrm{U_p} = \frac{\mathrm{I}/\mathrm{I_{at}}}{4\omega_L^2},$$

$$\mathrm{I_{at}} = 3.51 \times 10^{16}\ \mathrm{W/cm^2}.$$

ADB et al,J Mod Opt 52,411(2005)

(Vo > 0)

Semi-classical model, by P. Corkum (1993).

(Vo =0)

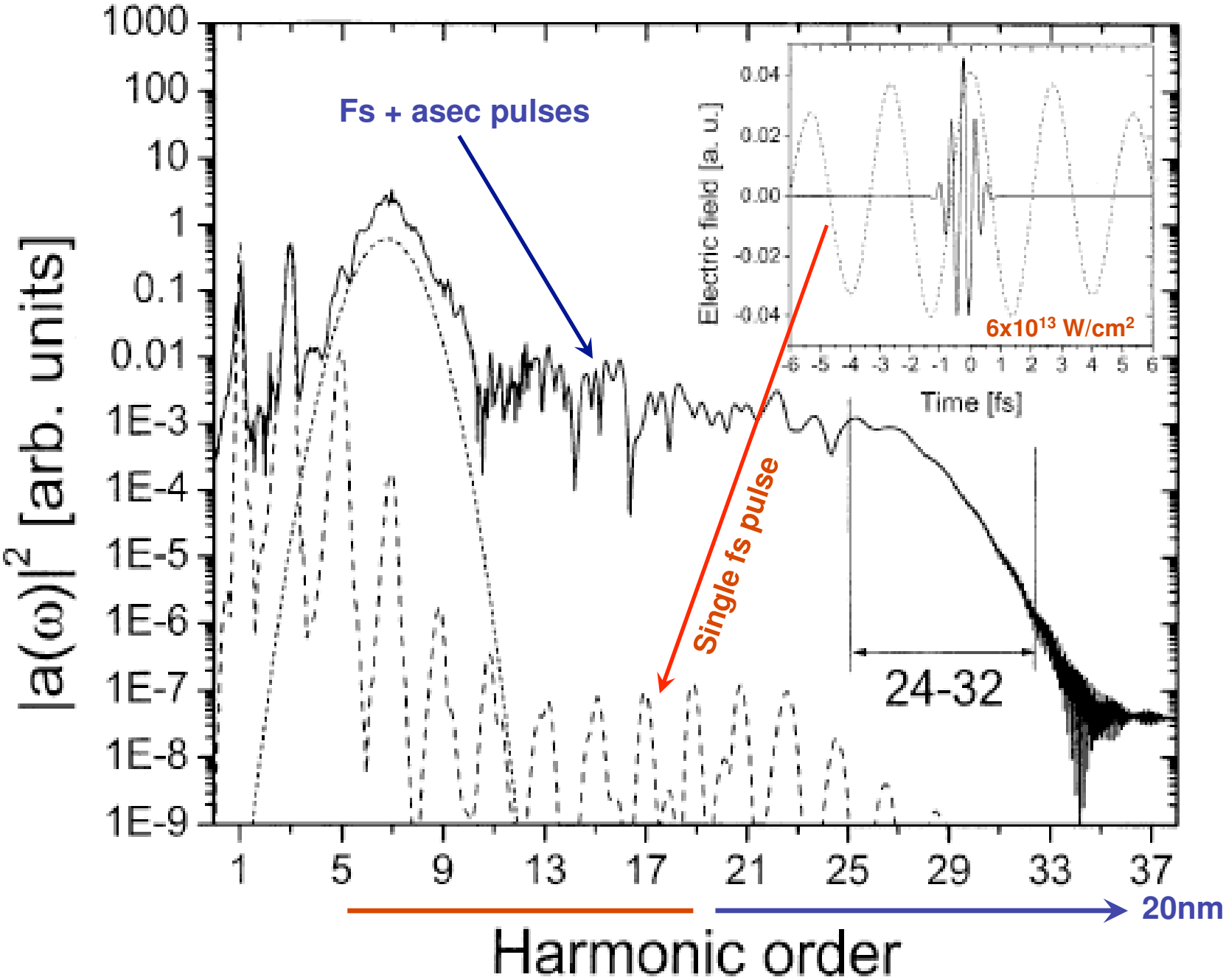
Fs + asec pulses
Single fs pulse
24-32
6x10^13 W/cm^2
Electric field [a. u.]
Time [fs]
|a(ω)|^2 [arb. units]
Harmonic order
20nm

Step 1: get spectrum

$$a(t) = \langle \psi(t) | -\delta H / \delta r | \psi(t) \rangle$$

$$a(\omega) = \frac{1}{2\pi} \int_{-\infty}^{+\infty} a(t) e^{-i\omega t} dt$$

Step2: select frequency region between $\omega_1 < \omega < \omega_2$

Step3: come back to time domain

$$\tilde{a}(t) = \int_{\omega_1}^{\omega_2} a(\omega) e^{i\omega t} d\omega$$

$$\Delta\omega = \omega_2 - \omega_1$$

$$\tau \quad \frac{1}{\Delta\omega} \rightarrow \text{attosecond}$$

= 3 Angstroms(10-8cm) / c(3x10**10cm/s-1))**

Model

Coupling of macroscopic Maxwell's equations with many TDSE's.

Lorin, Chelkowski, Bandrauk, Comput. Phys. Comm. vol. 177 (2007)

$$
\begin{cases}
\partial_t \mathbf{B}(\mathbf{r},t) & = & -\nabla \times \mathbf{E}(\mathbf{r},t) \\
\partial_t \mathbf{E}(\mathbf{r},t) & = & \nabla \times \mathbf{B}(\mathbf{r},t) - 4\pi \partial_t \mathbf{P}(\mathbf{r},t) \\
\nabla \cdot \mathbf{B}(\mathbf{r},t) & = & 0 \\
\nabla \cdot \big(\mathbf{E}(\mathbf{r},t) + \mathbf{P}(\mathbf{r},t)\big) & = & 0 \\
\\
\mathbf{P}(\mathbf{r},t) = n(\mathbf{r}) \sum_{i=1}^{m} \mathbf{P}_i(\mathbf{r},t) & = & n(\mathbf{r}) \sum_{i=1}^{m} \chi_{\Omega_i}(\mathbf{r}) \int_{\mathbb{R}^3} \psi_i \mathbf{r}' \psi_i^* \\
\mathtt{i}\partial_t \psi_i(\mathbf{r}',t) & = & -\frac{\triangle_{\mathbf{r}'}}{2}\psi_i + \mathbf{r}' \cdot \mathbf{E}_{\mathbf{r}_i}\psi_i + V_c \psi_i, \\
 & & \forall i \in \{1, ..., m\}
\end{cases}
$$

The numerical model is the one presented in [19], where the gas domain is divided in small cells of gas denoted by Δv (corresponding the Ω_i's of Section 2) and in which we solve 1 TDSE, representing the $n\Delta v$ molecules of the cell. In practice 3d Maxwell's equations are solved in parallel with $\sim 140,000$ 1d TDSE's, see Fig. 5 and [17]. We then represent at

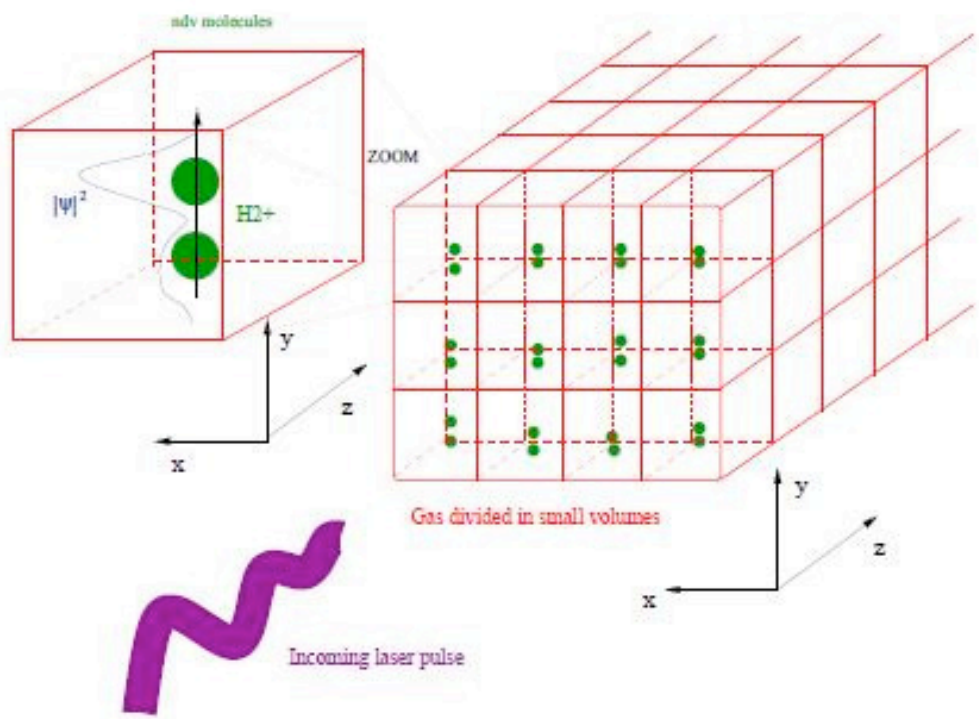

Figure 5: Numerical geometry

Improvement of the model I - microscopic approach

Another approach is presented in Lorin, Bandrauk, Chelkowski, Num. Methods for Partial Diff. Eq., (2008). A method to transmit free electron from a molecule to another. Based on a particular choice of boundary conditions (Volkov)

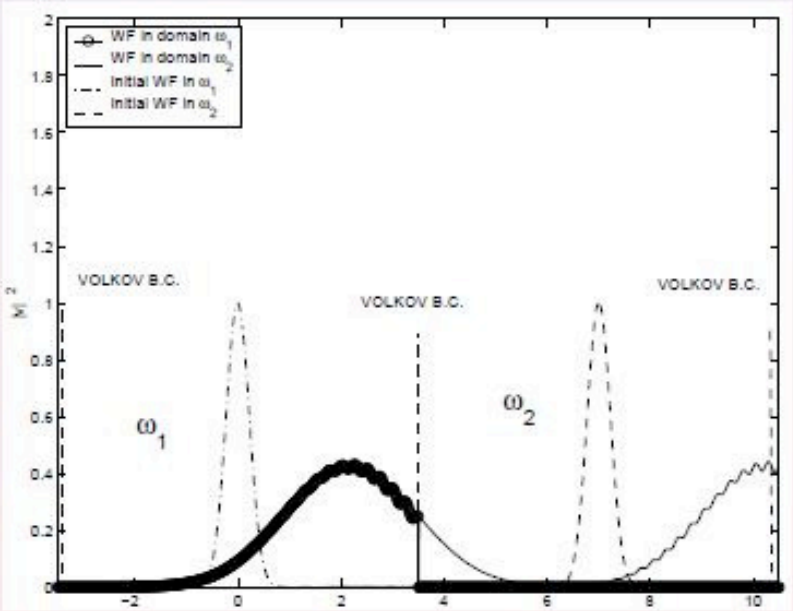

Figure: Free electron transmission

Results I - $I \sim 2 \times 10^{16} \mathrm{W{\cdot}cm^{-2}}$, $n_0 \sim 3 \times 10^{20} \mathrm{mol{\cdot}cm^{-3}}$

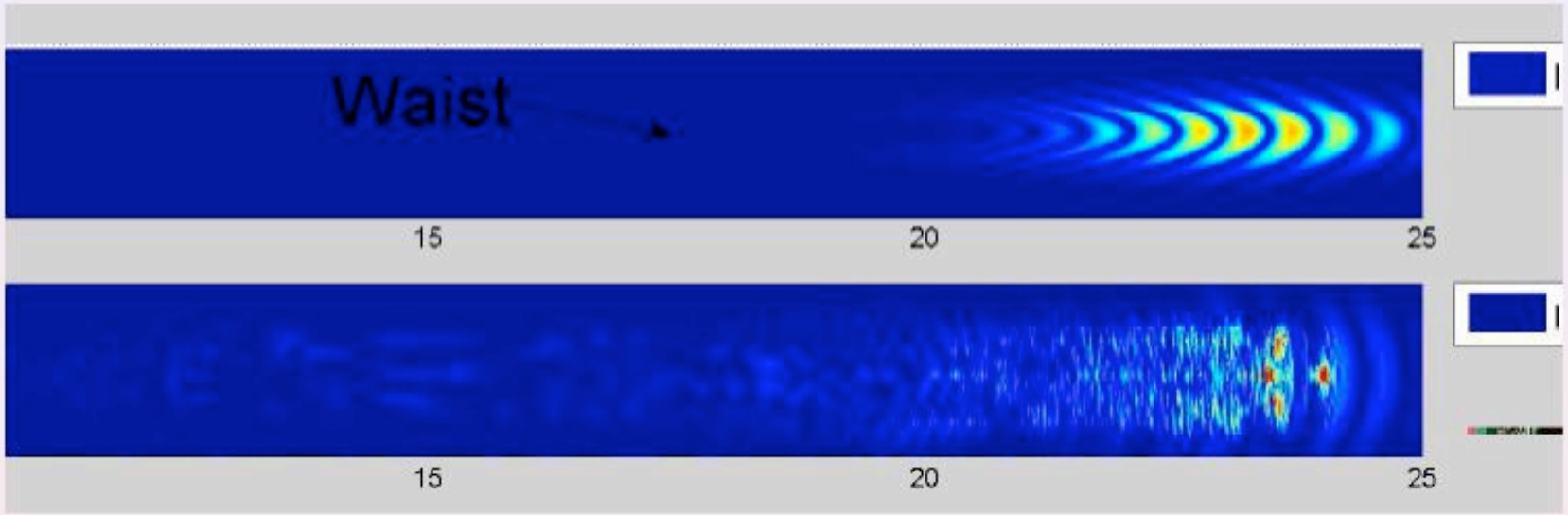

Figure: $|E_y|^2$ - $4.5\mu m$ after the waist in vacuum and gas

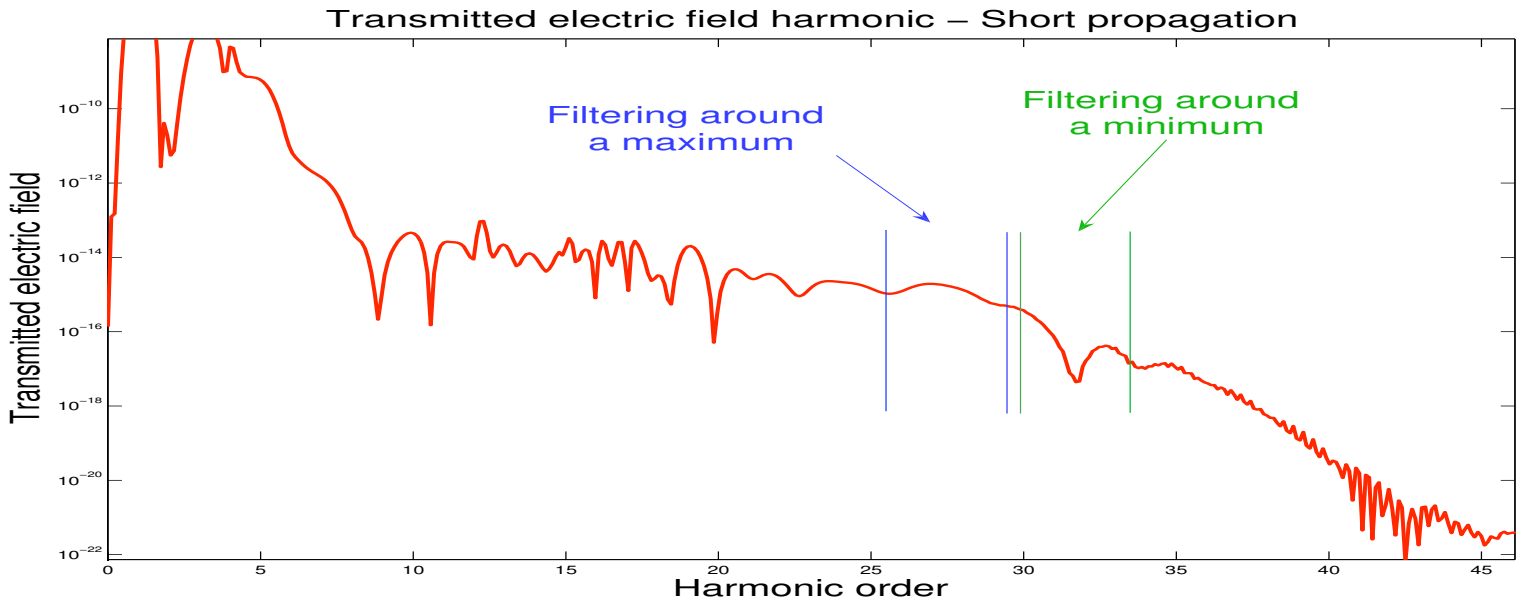

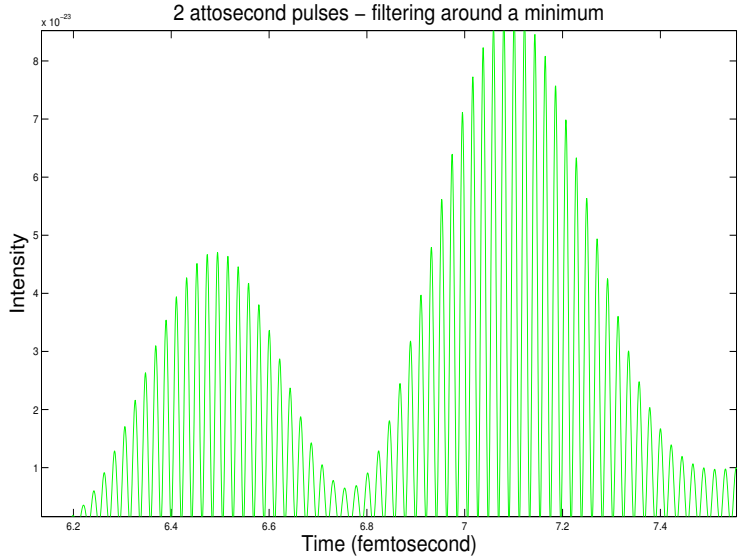

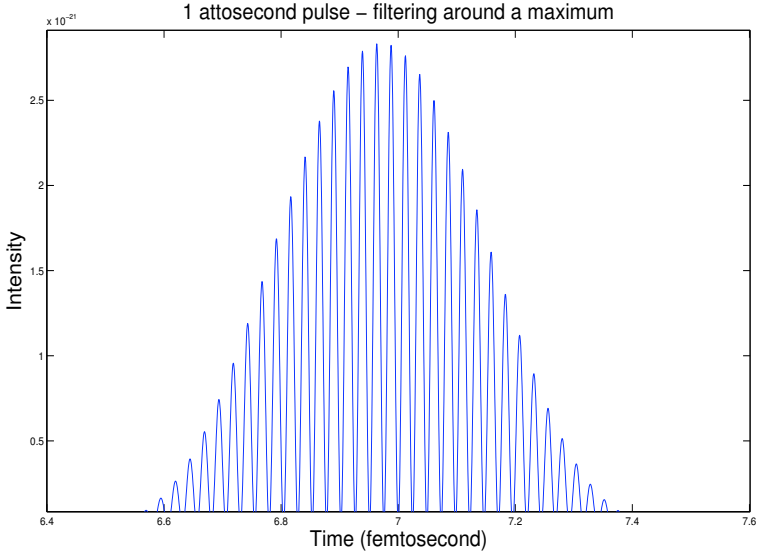

Two (minimum) or one (maximum) attosecond pulses

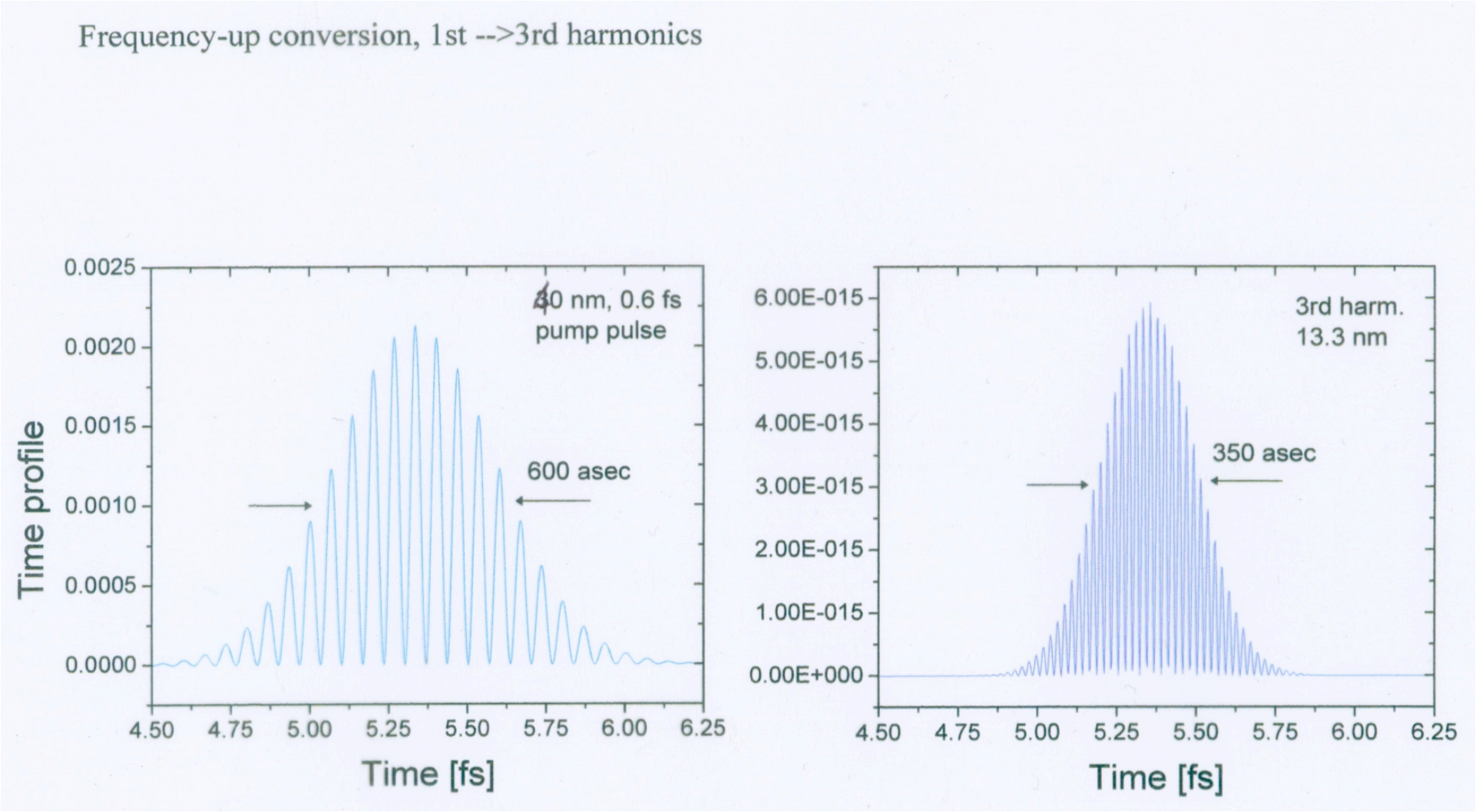

ADB et al,J Molec Str. 735,203(2004)

Goulielmakis,Krausz (2009-2010)

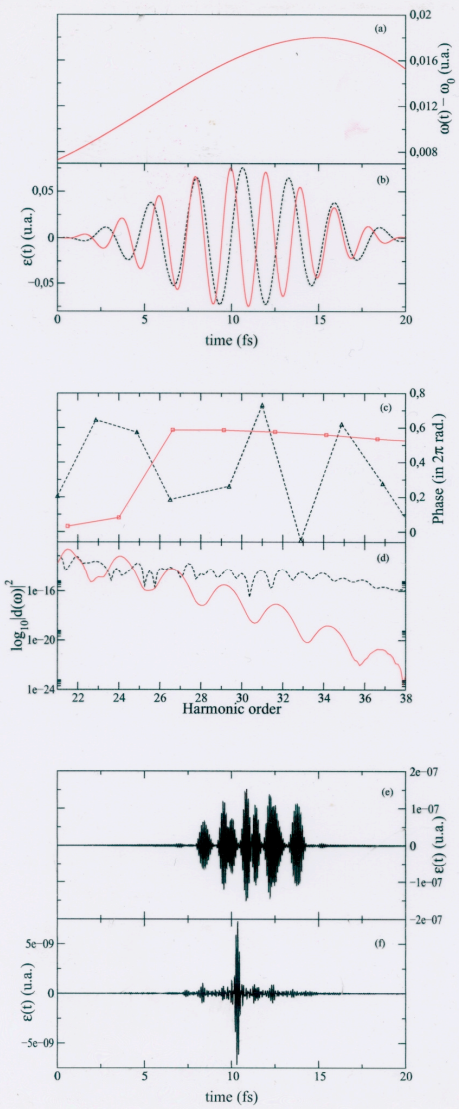

Yedder, LeBris, Chelkowski, Bandrauk, PRA 69, 041802 (2004)

((Bartels.Murrnane.Rabitz.PRA 70.043404(2004))

LQ11676

Effect of Nuclear Motion on Molecular High-order Harmonics and on Generation of Attosecond Pulses in Intense Laser Pulses

André D. Bandrauk, Szczepan Chelkowski, Shinnosuke Kawai, and Huizhong Lu

Département de Chimie, Université de Sherbrooke, Sherbrooke, Qc, J1K 2R1 Canada

Abstract

We calculate harmonic spectra and shapes of attosecond pulse trains using numerical solutions of Non-Born Oppenheimer time-dependent Shrödinger equation for 1-D H_2 molecules in an intense laser pulse. A very strong signature of nuclear motion is seen in the time profiles of high order harmonics. In general the nuclear motion shortens the part of the attosecond pulse train originating from the first electron contribution but it may enhance the second electron contribution for longer pulses. The shape of time profiles of harmonics can thus be used for monitoring the nuclear motion.

PACS numbers: 42.65.Ky, 42.65.Re, 42.50.Hz, 32.80.Rm

Phys Rev Lett(2008,)101,153901

J Phys B 42,075602 (2009)

La dynamique de 4-particules: $p+p+e^- +e^-$ décrite par l'éq. de Schrödinger solutionneé numé-riquement

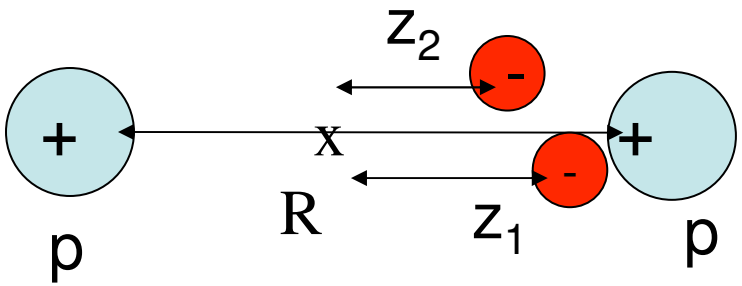

Équation de Schrödinger dependant de temps pour une molecule H_2

éxposée au champ laser intense decrit par : $E(t)=\varepsilon(t)\cos(\omega_L t)$

(polarisation linéaire)

a.u. $e = \hbar = m_e = 1$)

$$i\frac{\partial\psi(z_1,z_2,R,t)}{\partial t} = [H_e + H_N + V(z_1,z_2,t)]\psi(z_1,z_2,R,t), \qquad (1)$$

$$H_e = \sum_{i=1}^{2}[-\frac{1}{2}\frac{\partial^2}{\partial z_i^2} - \frac{1}{[(z_i+R/2)^2+c]^{1/2}} - \frac{1}{[(z_i-R/2)^2+c]^{1/2}}] + V_{rep}(z_1,z_2) \qquad (2)$$

$$V_{rep}(z_1,z_2) = \frac{1}{[(z_1-z_2)^2+d]^{1/2}} \;\; , \; ; H_N = -\frac{1}{2M}\frac{\partial^2}{\partial R^2} + \frac{1}{R} \qquad (3)$$

$$V(z_1,z_2,t) = (z_1+z_2)\varepsilon(t)\cos(\omega_L t) \qquad (4)$$

$$d(t)=\langle z_1+z_2\rangle = \int_{-\infty}^{\infty} dz_1 \int_{-\infty}^{\infty} dz_2 \int_{0}^{\infty} dR \; \psi^*(t)\,(z_1+z_2)\,\psi(t)$$

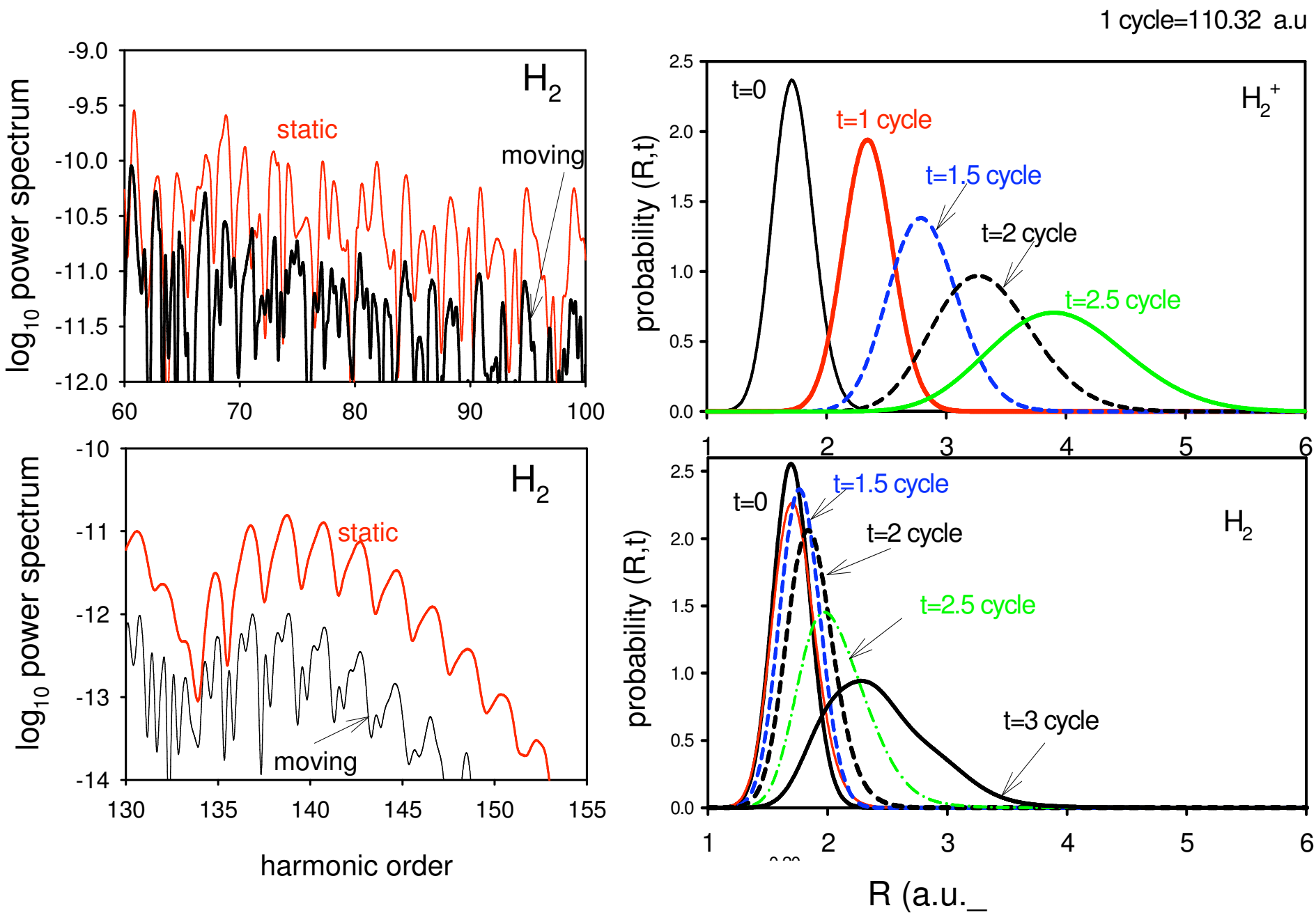
1 cycle=110.32 a.u
H2
static
moving
log10 power spectrum
harmonic order
H2+
t=0
t=1 cycle
t=1.5 cycle
t=2 cycle
t=2.5 cycle
probability (R,t)
H2
t=3 cycle
R (a.u._

Analyse en temps-frequence de Gabor (ondelettes):

$$= d_G(t,\omega) = \int_{-\infty}^{\infty} dt'\, G(t,t')\, \exp(-i\omega t)\, d(t)$$

$$G(t-t') = \exp[-\frac{(t-t')^2}{2\sigma_0^2}]\,, \quad \sigma_0 = 0.1 \text{ fs}$$

$$d_G(t,\omega) = \text{cte} \int_{-\infty}^{\infty} d\omega'\, e^{-b(\omega-\omega')^2}\, e^{i\omega' t}\, d_F(\omega')$$

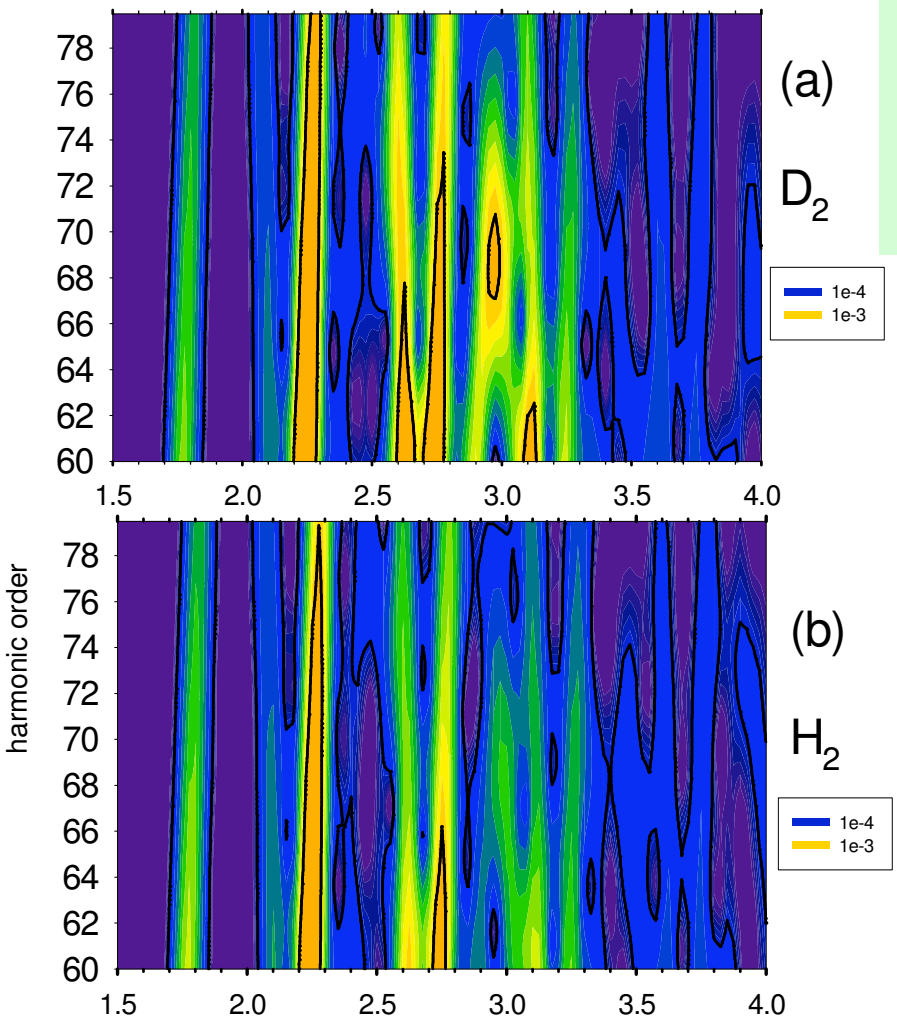

$|d_G(t,\omega)|$ - profile temporaire des impulsions atto dans un train , $\Delta\omega$~5-10 ω_L

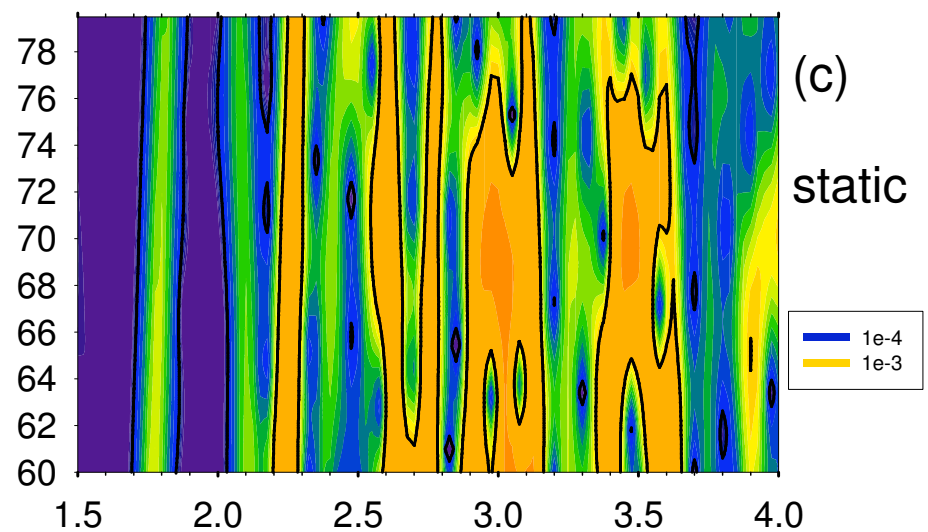

temps (periodes du laser T_{las}) , T_{las}=2.67 fs

Tv(H2) ~ 7 fs

$$V = \frac{1}{R} - \sum_{j=1}^{2} \frac{1}{\sqrt{(z_j - R/2)^2 + a}} + \frac{1}{\sqrt{(z_j + R/2)^2 + a}}$$

$$a_{el} = \frac{d^2}{dt^2} \overline{z(t)} = -2E(t) - < \frac{\partial V}{\partial z_1} + \frac{\partial V}{\partial z_2} >= -2E(t) - < F_+ + F_- >$$

$$a_R = \frac{d^2}{dt^2} \overline{R(t) =} -< \frac{1}{R^2} > - < \frac{\partial V}{\partial R} >= -< \frac{1}{R^2} > - \frac{1}{2} < F_+ - F_- >$$

where

$$F_\pm = \sum_{j=1}^{2} \frac{z_j \pm R/2}{[(z_j \pm R/2)^2 + a]^{3/2}}$$

Thus, very similar expressions determine electron and proton acceleration. For electrons:

$F_+ + F_- = f_{el}(z_1, z_2)$ is an odd function with respect to the inversion

$z_1 \to -z_1,\ z_2 \to -z_2$ leading to odd harmonics, whereas for protons

$F_+ - F_- = f_{prot}(z_1, z_2)$ is an even function with respect to the inversion

$z_1 \to -z_1,\ z_2 \to -z_2$ leading to even harmonics.

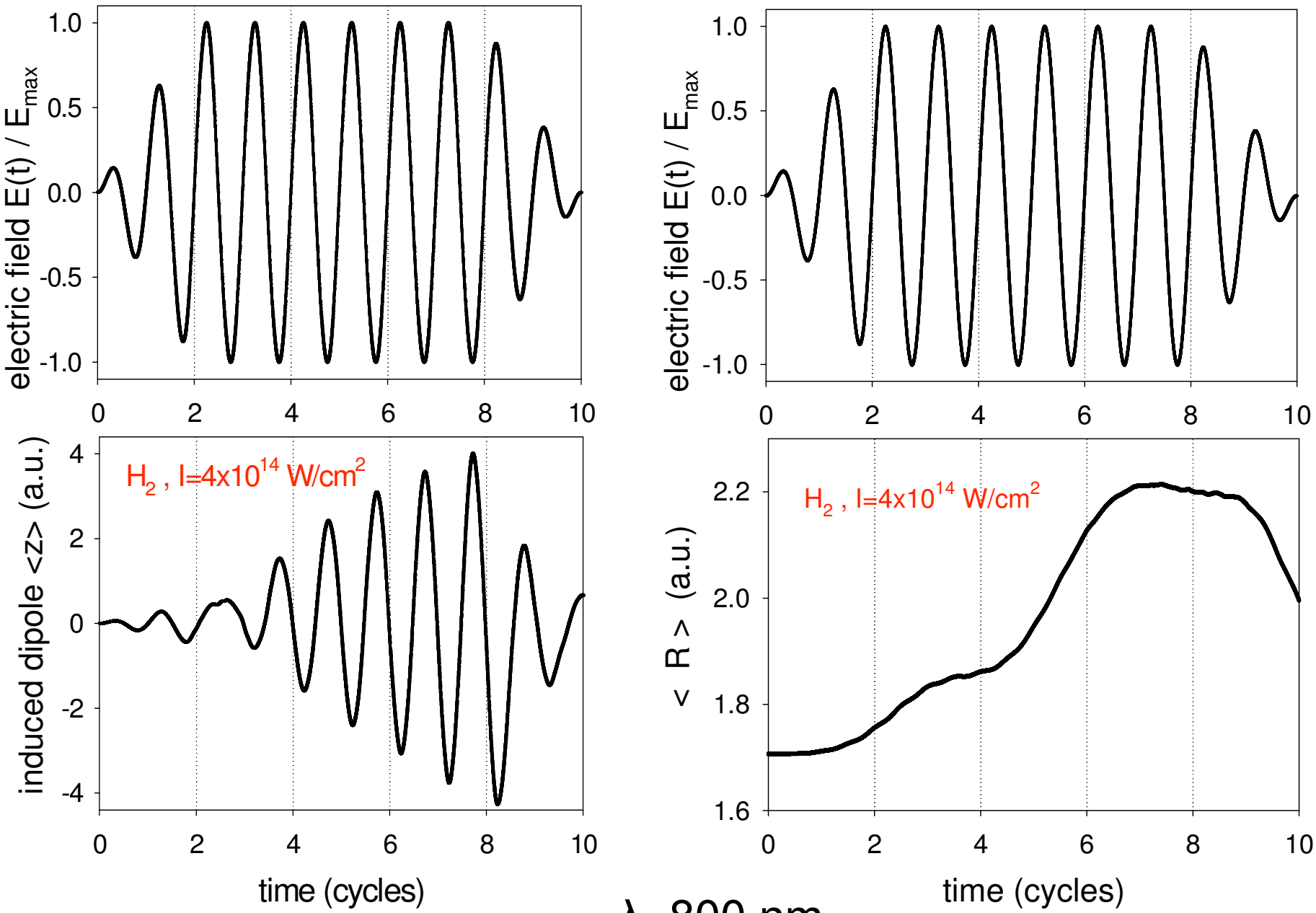
electric field E(t) / E_max
1.0
0.5
0.0
-0.5
-1.0
0
2
4
6
8
10
H2 , I=4x10^14 W/cm^2
induced dipole <z> (a.u.)
4
2
0
-2
-4
time (cycles)
< R > (a.u.)
2.2
2.0
1.8
1.6

λ=800 nm

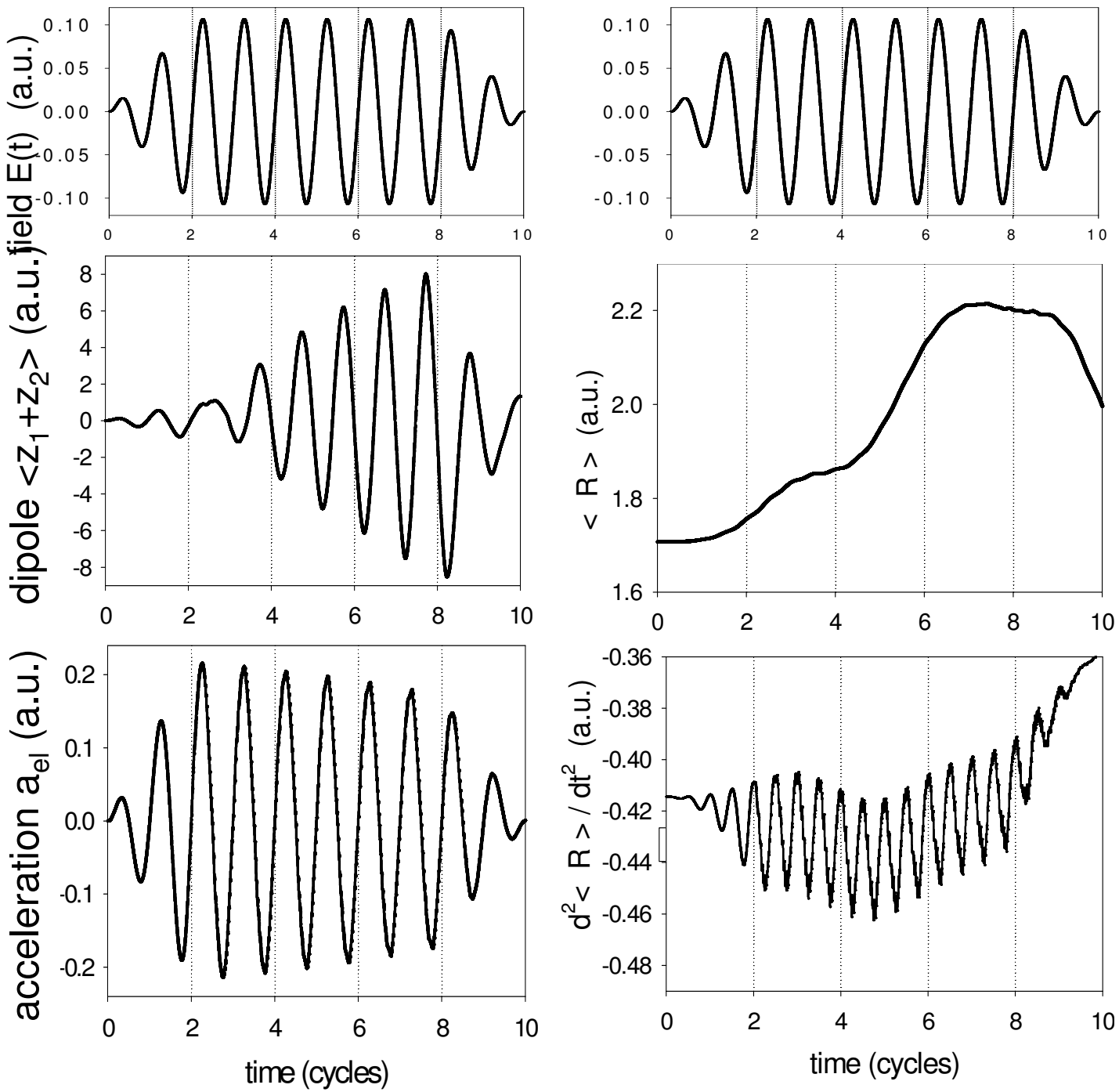
field E(t) (a.u.)
dipole <z1+z2> (a.u.)
acceleration ael (a.u.)
< R > (a.u.)
d2< R > / dt2 (a.u.)
time (cycles)
time (cycles)

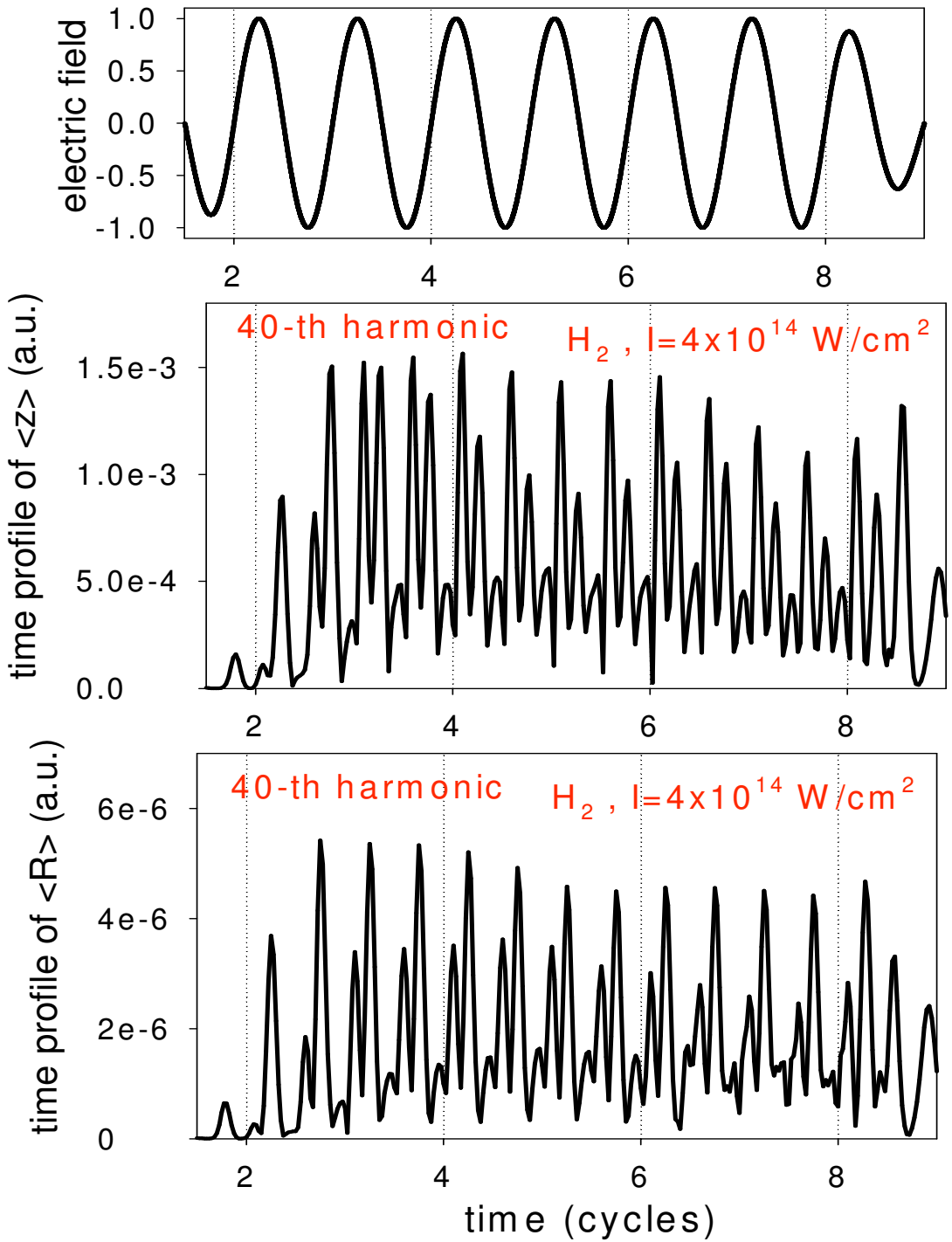
electric field
1.0
0.5
0.0
-0.5
-1.0
2
4
6
8
40-th harmonic
H2 , I=4x10^14 W/cm^2
time profile of <z> (a.u.)
1.5e-3
1.0e-3
5.0e-4
0.0
40-th harmonic
H2 , I=4x10^14 W/cm^2
time profile of <R> (a.u.)
6e-6
4e-6
2e-6
0
time (cycles)

λ=800 nm

To exploit attosecond technology

FP1

Measuring electron wave packets

1. Attosecond pulses are fast enough to observe electron wave packets.
2. Electron wave packets are resolved through changes to the photo-electron spectrum as a function of pump-probe time delay.
3. The attosecond pulse projects the momentum distribution into the continuum.

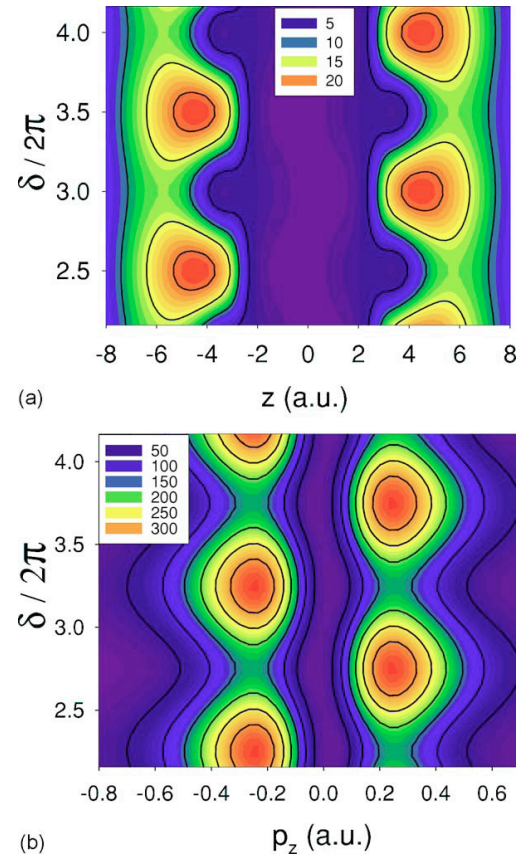

Yudin et al, Phys Rev A 72, 51401(R) (2005)

"Observing Electron Motion in Molecules"
SChelkowski,ADB J. Phys. B39, S409 (2006)

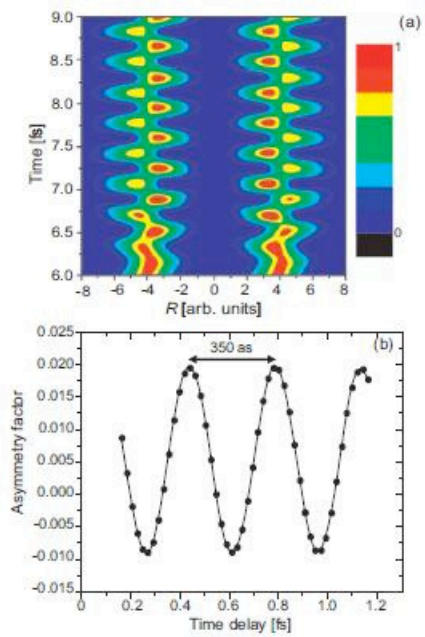

FIG. 53. (Color) Proposal for inducing attosecond electron wave-packet dynamics by a 0.8-fs, 115-nm VUV pump pulse in H_2^+ and probing it with a time-delayed 0.1-fs, 20-nm XUV pulse (Bandrauk *et al.*, 2004). Both pulses are polarized parallel to the molecular axis. (a) Contour plot of the electron probability distribution along the molecular axis for an internuclear distance of eight atomic units vs pump-probe delay. (b) Asymmetry factor $(P_- - P_+)/(P_- + P_+)$ vs delay, where P_+ and P_- represent the probability of observing the electron liberated by the XUV probe in the positive or negative direction (along the molecular axis), respectively. Adapted from Bandrauk *et al.*, 2004.

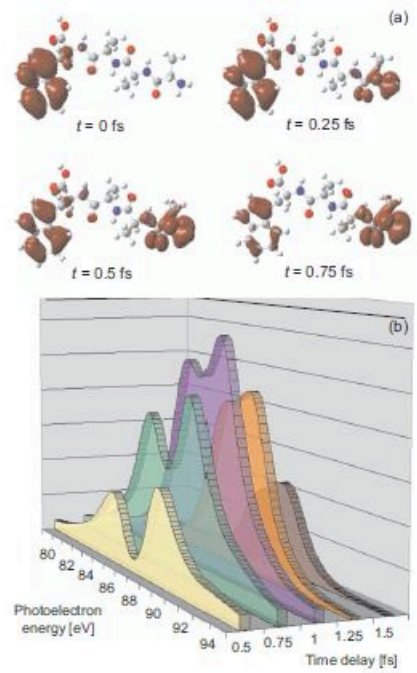

FIG. 54. (Color) Computed ultrafast positive charge (hole) migration in a tryptophane-terminated tetrapeptide (Remacle and Levine, 2006a, 2007). (a) The hole density shown in red indicates that the charge swings across the entire peptide from the aromatic amino acid on the left to the *N* end on the right within less than one femtosecond, following excitation of the electronic wave packet on an attosecond time scale. This hyperfast charge migration is proposed to be probed by measuring the kinetic energy distribution of photoelectrons released by a time-delayed sub-fs XUV pulse. (b) A series of such freeze-frame spectra calculated for a 250-as, 95-eV probe pulse at different pump-probe delays. From Remacle and Levine,

Rev Mod Phys, 81, 235 (2009)

Circular polarization Excitation at 800 nm I=10**14 W/cm2

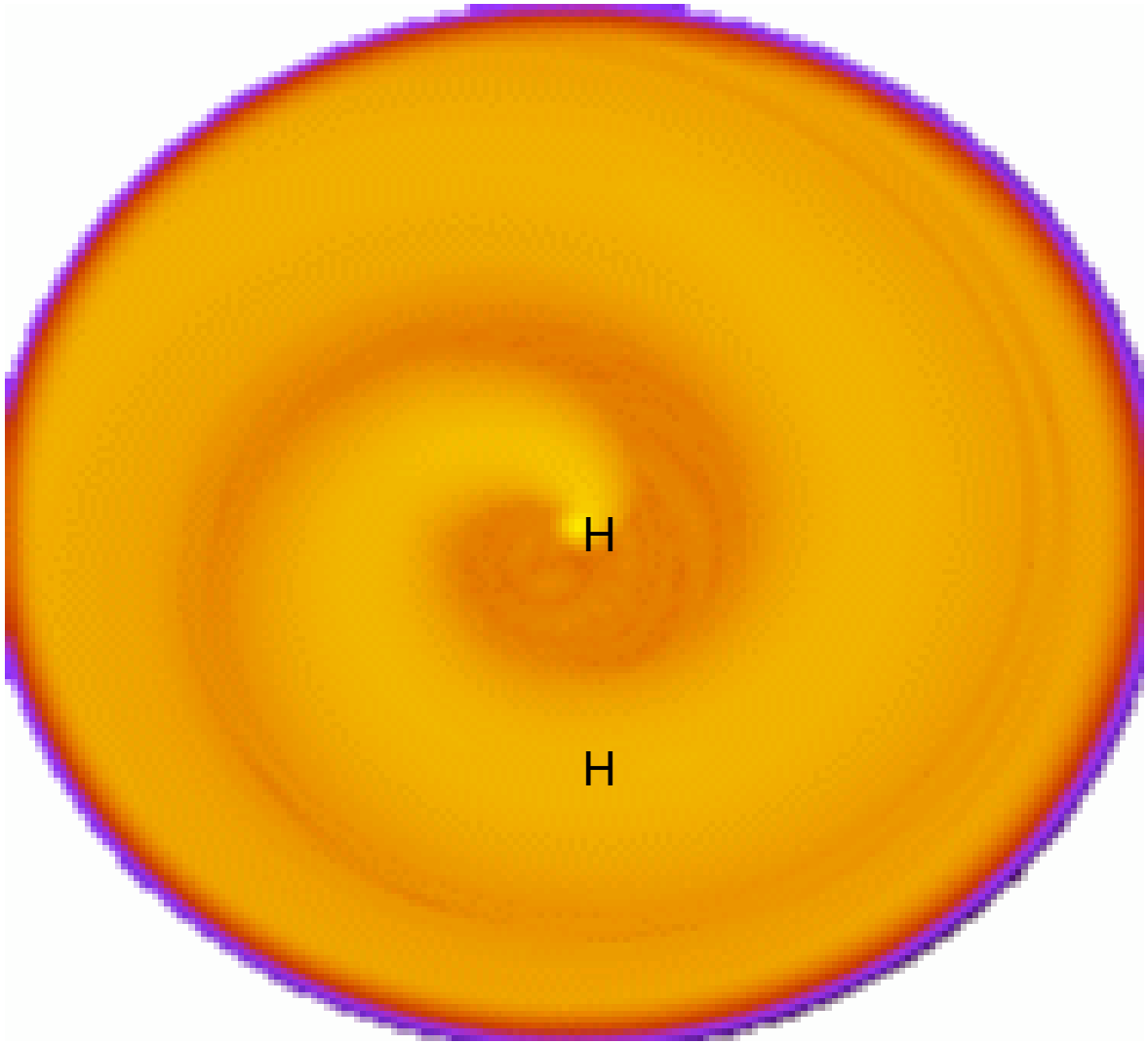

Electron Whirlpool – Tourbillon Electronique –
Elektronischer Wirbel (J Manz- FU Berlin)

II. THEORETICAL MODELS

In linearly polarized recollision with parent ions, maximum harmonic energies are given from the initial zero velocity ionization model by $I_p + 3.17U_p$ [3–6], whereas collision with neighboring ions gives harmonic energies up to $I_p + 8U_p$ [9–12]. For circularly polarized laser pulses of maximum amplitude E_0, corresponding to intensity $I_0 = c\varepsilon_0 E_0^2/2$ and frequency ω_0,

$$E_x(t) = E_0 \cos(\omega_0 t + \phi), \quad E_y(t) = E_0 \sin(\omega_0 t + \phi), \tag{1}$$

the classical field equations of motion [$\ddot{x}(t) = -E_x(t)$, $\ddot{y}(t) = -E_y(t)$] give the laser-induced velocities [we use atomic units (a.u.) $e = \hbar = m_e = 1$ throughout]

$$\begin{aligned} \dot{x}(t) &= -\frac{E_0}{\omega_0}[\sin(\omega_0 t + \phi) - \sin\phi], \\ \dot{y}(t) &= -\frac{E_0}{\omega_0}[\cos\phi - \cos(\omega_0 t + \phi)], \end{aligned} \tag{2}$$

with initial velocity conditions $\dot{x}(0) = \dot{y}(0) = 0$, and displacements,

$$\begin{aligned} x(t) &= -\frac{E_0}{\omega_0^2}[\cos\phi - \cos(\omega_0 t + \phi) - \omega_0 t \sin\phi], \\ y(t) &= -\frac{E_0}{\omega_0^2}[\omega_0 t \cos\phi + \sin\phi - \sin(\omega_0 t + \phi)]. \end{aligned} \tag{3}$$

Both the time-dependent energy from Eq. (2),

$$K_e(t) = \frac{1}{2}[\dot{x}^2(t) + \dot{y}^2(t)] \tag{4}$$

$$= \left(\frac{E_0}{\omega_0}\right)^2 (1 - \cos\omega_0 t), \tag{5}$$

with maximum value $8U_p$ at $\omega_0 t_c = (2n+1)\pi$, where t_c is collision time, the ponderomotive energy of electron in circularly polarized laser fields $U_p = E_0^2/4\omega_0^2$, and the corresponding maximum electron displacement (transfer) to a neighboring ion from Eq. (3),

$$R_n = \sqrt{x^2(t_c) + y^2(t_c)} = \frac{2E_0}{\omega_0^2}\sqrt{1 + \left(n + \frac{1}{2}\right)^2 \pi^2}, \tag{6}$$

for integer n, are independent of the CEP, ϕ. For x-aligned molecules,

$$\begin{aligned} x(t_c) = R_n &= -\frac{2E_0}{\omega_0^2}\left[1 + \left(n + \frac{1}{2}\right)^2 \pi^2\right]\cos\phi, \\ y(t_c) &= 0, \end{aligned} \tag{7}$$

where $\tan\phi = -(n + \frac{1}{2})\pi$.

With a two-color circularly polarized laser field,

$$\begin{aligned} E_x(t) &= E_0[\cos(\omega_0 t + \phi_1) + \cos(2\omega_0 t + \phi_2)], \\ E_y(t) &= E_0[\sin(\omega_0 t + \phi_1) + \sin(2\omega_0 t + \phi_2)], \end{aligned} \tag{8}$$

the CEPs ϕ_1 and ϕ_2 determine the optimal values of $K_e(t)$ and $R(t)$ for MHOHG. The corresponding laser-induced velocities are

$$\begin{aligned} \dot{x}(t) &= -\frac{E_0}{\omega_0}[\sin(\omega_0 t + \phi_1) - \sin\phi_1 + \cos(\omega_0 t + \phi_2)\sin\omega_0 t], \\ \dot{y}(t) &= -\frac{E_0}{\omega_0}[\cos\phi_1 - \cos(\omega_0 t + \phi_1) + \sin(\omega_0 t + \phi_2)\sin\omega_0 t], \end{aligned} \tag{9}$$

and the displacements are

$$\begin{aligned} x(t) = -\frac{E_0}{4\omega_0^2}[&4\cos\phi_1 - 4\omega_0 t\sin\phi_1 - 4\cos(\omega_0 t + \phi_1) \\ &- \cos(2\omega_0 t + \phi_2) + \cos\phi_2 - 2\omega_0 t\sin\phi_2], \\ y(t) = -\frac{E_0}{4\omega_0^2}[&4\sin\phi_1 + 4\omega_0 t\cos\phi_1 - 4\sin(\omega_0 t + \phi_1) \\ &- \sin(2\omega_0 t + \phi_2) + \sin\phi_2 + 2\omega_0 t\cos\phi_2]. \end{aligned} \tag{10}$$

Maximizing kinetic energy K_e with respect to ϕ_1 and ϕ_2 gives the net optimal CEP condition $\phi = \phi_1 - \phi_2 = n\pi + \omega_0 t/2$. Inserting this condition into K_e, Eq. (4), and maximizing the resulting K_e with respect to $\omega_0 t_c$ gives the result for $n = 0$, $\omega_0 t_c = 2\pi/3$, and $\phi = \pi/3$, whereas for $n = 1$, $\omega_0 t_c = 4\pi/3$, and $\phi = -\pi/3$.

For $n = 0$ the choice of phases $\omega_0 t_c = 2\pi/3$ and $\phi = \phi_1 - \phi_2 = \pi/3$ $(n = 0)$ gives, respectively, the following components of K_e, where $U_p = E_0^2/4\omega_0^2$:

$$\begin{aligned} K_{ex} &= \frac{1}{2}\dot{x}^2(t_c) = \frac{9}{32}\left(\frac{E_0}{\omega_0}\right)^2(\sqrt{3}\cos\phi_2 + 3\sin\phi_2)^2, \\ K_{ey} &= \frac{1}{2}\dot{y}^2(t_c) = \frac{9}{32}\left(\frac{E_0}{\omega_0}\right)^2(3\cos\phi_2 - \sqrt{3}\sin\phi_2)^2, \\ K_e &= K_{ex} + K_{ey} = \frac{1}{2}[\dot{x}^2(t_c) + \dot{y}^2(t_c)] = 13.5U_p. \end{aligned} \tag{11}$$

The second choice for $n = 1$, $\omega_0 t_c = 4\pi/3$ and $\phi = \phi_1 - \phi_2 = -\pi/3$, corresponds to replace ϕ_2 by $-\phi_2$ in Eq. (11). Equation (11) shows that the total K_e is independent of ϕ_2 for both optimal CEPs $\phi = \pm\pi/3$. In Figs. 1(a) and 1(b) we show K_e as a function of ϕ_1 and ϕ_2. Maximum $K_e = 13.5U_p$ occurs for $\phi_1 = \pm\pi/3 + \phi_2$ as predicted by Eq. (11). However, the different velocities and displacements are functions of ϕ_2 [Figs. 1(c)–1(f)]. We show an unusual symmetry in Figs. 1(c) and 1(d) for $\phi = +\pi/3$ and $-\pi/3$. The corresponding x and y components of K_e alternate in phase.

At intensity $I_0 = 2 \times 10^{14}$ W/cm^2 ($E_0 = 0.0755$ a.u.) and $\lambda = 400$ nm ($\omega_0 = 0.114$ a.u.), the electron displacements (transfer distances) $x(t_c)$ and $y(t_c)$ for $\omega_0 t_c = 2\pi/3$ and $\phi = \pi/3$ $(n = 0)$ and for $\omega_0 t_c = 4\pi/3$ and $\phi = -\pi/3$ $(n = 1)$ are shown in Figs. 1(e) and 1(f), respectively. With $\omega_0 t_c = 2\pi/3$, for example, for phases $\phi_1 = \pi/3$ and $\phi_2 = 0$, the electron displacements are $x(t_c) = -0.35$ a.u. and $y(t_c) = -18.5$ a.u. and for $\phi_1 = 0$ and $\phi_2 = -\pi/3$, the electron displacements are $x(t_c) = -16.2$ a.u. and $y(t_c) = -8.9$ a.u. from Eq. (10). Maximum efficiency of the MHOHG process is obtained for the smallest $x(t_c)$ or $y(t_c)$ which corresponds to near direct (head-on) collision with a neighboring nucleus. Thus at $\lambda = 800$ nm ($\omega_0 = 0.057$ a.u.), the corresponding electron displacements are, respectively, $x(t_c) = -1.4$ a.u. and $y(t_c) = -74$ a.u. and $x(t_c) = -64.6$ a.u. and $y(t_c) = -35.7$ a.u. We conclude hence that short wavelengths (e.g., $\lambda = 400$ nm) and

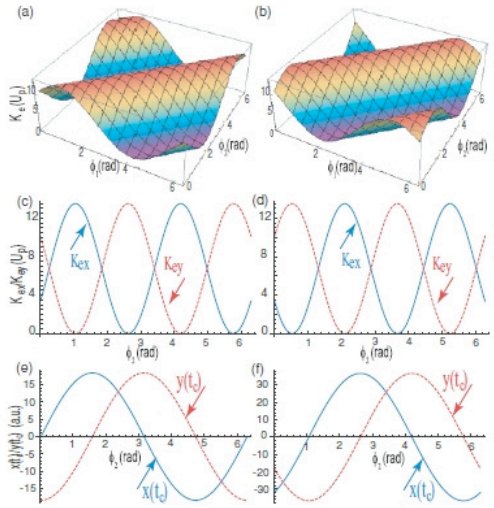

FIG. 1. (Color online) Total kinetic K_e as a function of phases ϕ_1 and ϕ_2 (radian) for the cases (a) $n = 0$ and $\omega_0 t_c = 2\pi/3$ and (b) $n = 1$ and $\omega_0 t_c = 4\pi/3$. The CEPs $\phi = \phi_1 - \phi_2 = \pi/3$ and $\phi = -\pi/3$ give the maximum $K_e = 13.5U_p$, respectively. The corresponding kinetic energies K_{ex} and K_{ey}, Eq. (11) (c–d), and displacements $x(t_c)$ and $y(t_c)$, Eq. (10) (e–f), for the maximum K_e with a bichromatic circularly polarized laser pulse at $I_0 = 2 \times 10^{14}$ W/cm^2 ($E_0 = 0.0755$ a.u.), $\lambda_1 = 400$ nm ($\omega_0 = 0.114$ a.u.), and $\lambda_2 = 200$ nm ($\omega_0 = 0.228$ a.u.) as a function of ϕ_2.

phases $\phi_1 = \pi/3$ and $\phi_2 = 0$ give the best collision conditions with neighboring ions, thus increasing MHOHG efficiencies.

III. COMPUTATIONAL METHODS

We consider the H_2^+ molecular ion at a fixed internuclear separation R (Born-Oppenheimer approximation) interacting with a circularly polarized laser pulse $\mathbf{E}(t)$. The corresponding 2D (plane) TDSEs

$$i\frac{\partial}{\partial t}\Psi(\mathbf{r},t) = H(\mathbf{r},t)\Psi(\mathbf{r},t), \tag{12}$$

$$H(\mathbf{r},t) = H_0(\mathbf{r}) + \mathbf{r}\cdot\mathbf{E}(t), \tag{13}$$

$$H_0(\mathbf{r}) = -\tfrac{1}{2}\nabla_{\mathbf{r}}^2 + V(\mathbf{r}), \tag{14}$$

where $r = x$ and y, $V(\mathbf{r})$ is the two-center Coulomb potential, and the matter-field interaction is treated in the length gauge, are solved numerically by a three-point difference combined with higher-order split-operator methods [26,27]. A temporal slowly varying envelope $\sin^2(\pi t/10\tau)$, where one optical cycle (o.c.) $\tau = 2\pi/\omega_0$, is adopted. The MHOHG power spectrum $P_r(\omega)$ is obtained from the absolute square of the Fourier transforms (FT) of the dipole acceleration $\langle\ddot{r}(t)\rangle$:

$$P_r(\omega) = \left|\int \exp(-i\omega t)\langle\ddot{r}(t)\rangle dt\right|^2 \tag{15}$$

with the laser-induced electron acceleration obtained from the exact time-dependent electron wave function $\Psi(\mathbf{r},t)$,

$$\langle\ddot{r}(t)\rangle = \langle\Psi(\mathbf{r},t)| - \partial H(\mathbf{r})/\partial r|\Psi(\mathbf{r},t)\rangle. \tag{16}$$

For the ten-optical-cycles pulse used here, the HHG spectra calculated from the FT of dipole moment, velocity, and acceleration forms give nearly the same results [28].

To describe the polarization properties of the emitted MHOHG [29], the relevant physical quantities are introduced (see, for example, Fig. 1 in [22]). The complex integral in Eq. (15) has two x and y components, thus allowing us to extract the dependence of the phase difference δ between the polarized component of the emitted harmonics on the angular frequency ω [30]. The ellipticity ε and the orientation angle φ, the angle between the major axis of the ellipse and the y axis, are defined, respectively, as

$$\varepsilon = \tan\chi \tag{17}$$

and

$$\tan(2\varphi) = \tan(2\gamma)\cos\delta, \tag{18}$$

where

$$\sin(2\chi) = \sin(2\gamma)\sin\delta, \tag{19}$$

$$\tan\gamma = \sqrt{P_x/P_y}. \tag{20}$$

IV. NUMERICAL RESULTS AND DISCUSSIONS

The numerical results in Fig. 2 based on solutions of the x-aligned H_2^+ TDSE, Eqs. (12)–(14), with a single circularly polarized laser pulse confirm our conclusion in Eq. (5) where maximum harmonic energy $I_p + 8U_p$ is induced. For wavelength $\lambda = 400$ nm ($\omega_0 = 0.114$ a.u.) and intensity $I_0 = 2.1 \times 10^{14}$ W/cm^2 ($E_0 = 0.077$ a.u.), Fig. 2 shows the corresponding MHOHG spectrum at the internuclear distance $R = 22$ a.u. corresponding to $R_n = 3.72E_0/\omega_0^2$, Eq. (6) with $n = 0$. The maximum harmonic order $N_m = (I_p + 8U_p)/\omega_0$

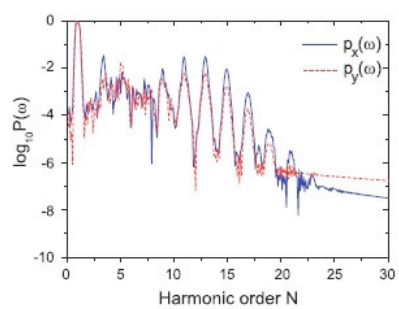

FIG. 2. (Color online) The x (solid blue line) and y (dashed red line) components of x-aligned H_2^+ MHOHG at $R = x(t_c) = 22$ a.u. for $\lambda = 400$ nm, $I_0 = 2.1 \times 10^{14}$ W/cm^2, and $\phi = \tan^{-1}(-\pi/2)$ circularly polarized light. The cutoff order $N_m = (I_p + 8U_p)/\omega_0 \approx 13$.

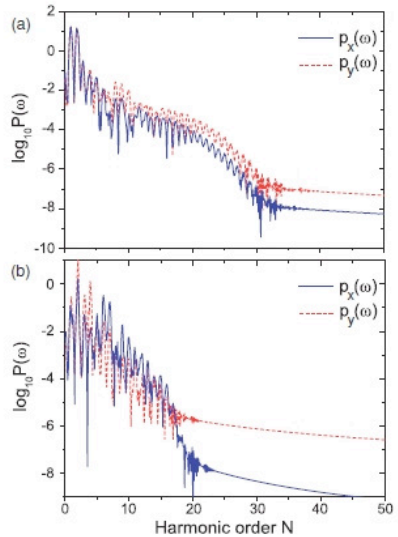

FIG. 3. (Color online) MHOHG spectra of y-aligned H_2^+ with a bichromatic circularly polarized laser pulse at $I_0 = 2 \times 10^{14}$ W/cm^2, $\lambda_1 = 400$ nm, $\lambda_2 = 200$ nm, $\phi_1 = \pi/3$, and $\phi_2 = 0$ (a) at $R = -y(t_c) = 19$ a.u. and (b) at $R_e = 2$ a.u. The cutoff order $N_m = (I_p + 13.5U_p)/\omega_0 \approx 18$ for $n = 0$, $\omega_0 t_c = 2\pi/3$, and $\phi = \phi_1 - \phi_2 = \pi/3$.

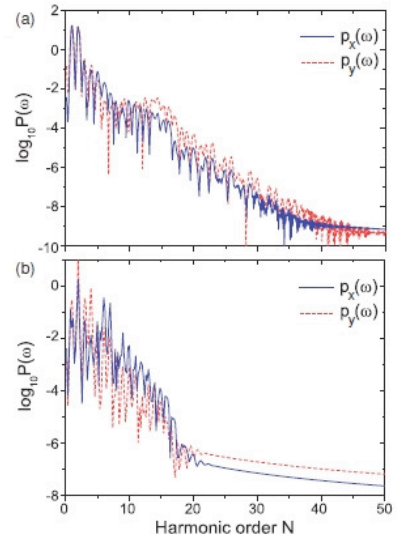

FIG. 4. (Color online) MHOHG spectra of y-aligned H_2^+ with a bichromatic circularly polarized laser pulse at $I_0 = 2 \times 10^{14}$ W/cm^2, $\lambda_1 = 400$ nm, $\lambda_2 = 200$ nm, $\phi_1 = 0$, and $\phi_2 = \pi/3$ (a) at $R = -y(t_c) = 37$ a.u. and (b) at $R = 2$ a.u. The cutoff order $N_m = (I_p + 13.5U_p)/\omega_0 \approx 18$ for $n = 1$, $\omega_0 t_c = 4\pi/3$, and $\phi = \phi_1 - \phi_2 = -\pi/3$.

occurs around $N_m = 13$ in both x and y directions, with a decrease in intensity for orders larger than N_m. We reemphasize that for equilibrium H_2^+ ($R_e = 2$ a.u.) *no* harmonics are appreciably produced and observed numerically and *none* for the H atom since the ionized electron never collides with the parent ion.

Figure 3(a) illustrates the MHOHG spectrum obtained for H_2^+ aligned with the y-axis such that $y(t_c) = -R = -19$ a.u. and $x(t_c) = -0.35$ a.u. at $I_0 = 2 \times 10^{14}$ W/cm^2 ($E_0 = 0.0755$ a.u.), $\lambda_1 = 400$ nm ($\omega_0 = 0.114$ a.u.), $\lambda_2 = 200$ nm ($2\omega_0 = 0.228$ a.u.), and $\phi_1 = \pi/3$ and $\phi_2 = 0$ ($\phi = \pi/3$). A plateau is obtained between harmonic orders 10 and 20 with a cutoff (decrease) around the harmonic energy $I_p + 13.5U_p$. Figure 4(a) shows, with the same pulses but phases $\phi_1 = 0$ and $\phi_2 = \pi/3$ ($\phi = -\pi/3$), a similar MHOHG spectrum obtained but $y(t_c) = -R = -37$ a.u. and $x(t_c) = -0.35$ a.u. at collision. In Fig. 5(a), at the same intensity but longer wavelengths $\lambda_1 = 800$ nm ($\omega_0 = 0.057$ a.u.) and $\lambda_2 = 400$ nm ($2\omega_0 = 0.114$ a.u.) and phases $\phi_1 = \pi/3$ and $\phi_2 = 0$ ($\phi = \pi/3$), the same maximum harmonic order is obtained: $N_m = (I_p + 13.5U_p)/\omega_0$ but now $y(t_c) = -R = -74$ a.u. and $x(t_c) = -1.4$ a.u. at collision with the neighbor. In Figs. 3(b), 4(b), and 5(b) we show the MHOHG spectrum at the equilibrium distance $R_e = 2$ a.u. We see the absence of a long plateau with high efficiencies since now collision with neighboring nuclei *does not* occur, but rather the H_2^+ molecule at $R_e = 2$ a.u. appears like a one-center atom to the ionized electron at larger x and y. We reemphasize that at

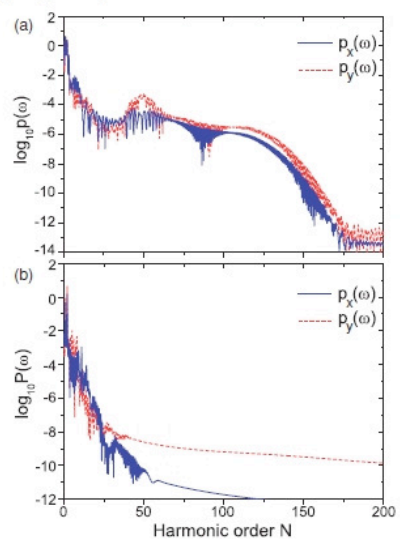

FIG. 5. (Color online) MHOHG spectra of y-aligned H_2^+ with a bichromatic circularly polarized laser pulse at $I_0 = 2 \times 10^{14}$ W/cm^2, $\lambda_1 = 800$ nm, $\lambda_2 = 400$ nm, $\phi_1 = \pi/3$, and $\phi_2 = 0$ (a) at $R = -y(t_c) = 74$ a.u. and (b) at $R_e = 2$ a.u. The cutoff order $N_m = (I_p + 13.5U_p)/\omega_0 \approx 120$ for $n = 0$, $\omega_0 t_c = 2\pi/3$, and $\phi = \phi_1 - \phi_2 = \pi/3$.

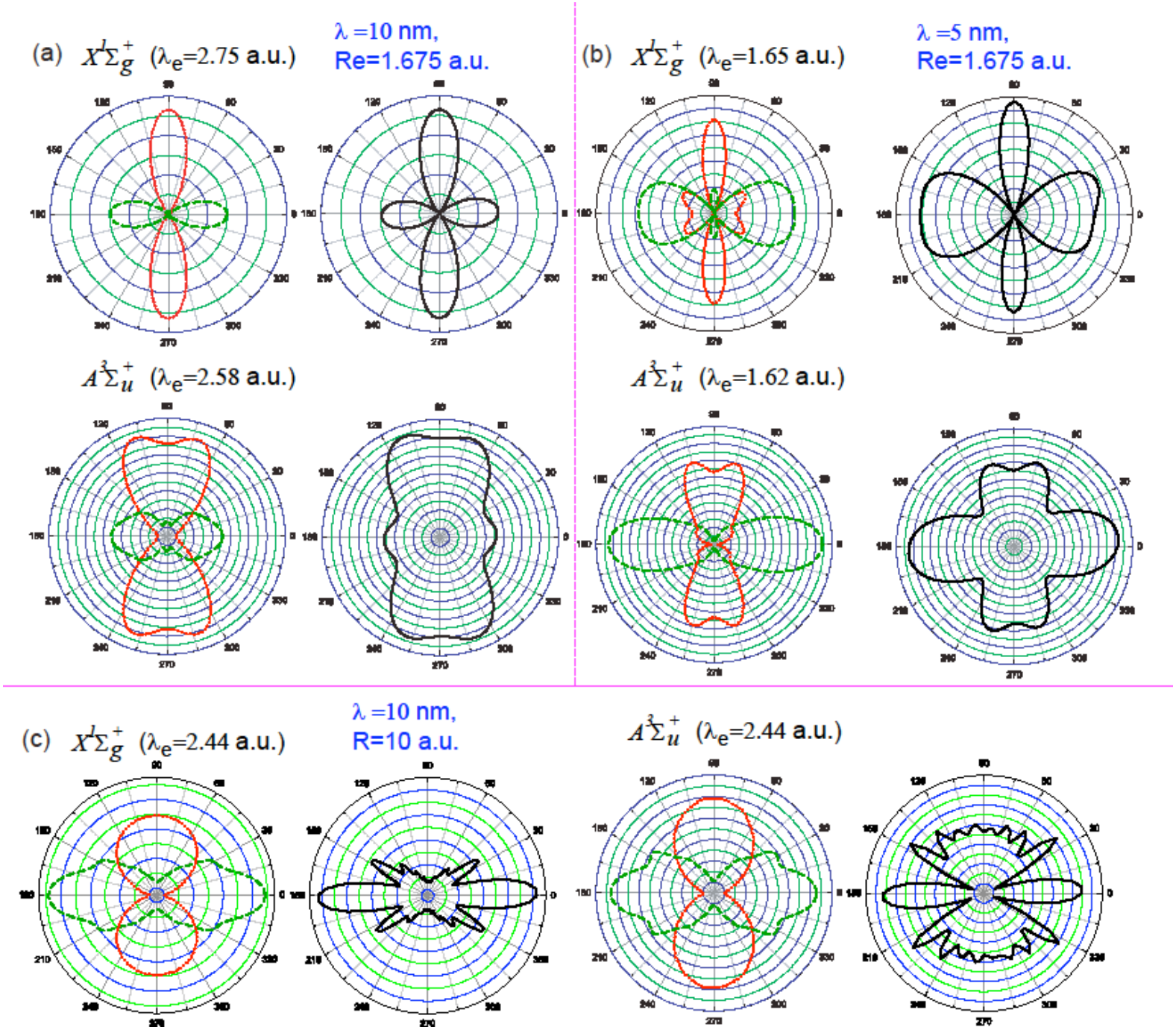

KJ Yuan & ADB..PRA 80.061403(2009) ..PRA 2011

ChemPhysChem, Volume 10, Issue 3 (p 493-494)

HIGHLIGHTS

DOI: 10.1002/cphc.200800770

The Molecular Cat

Maddalena Pedio[b] and Majed Chergui*[a]

One of the often-claimed advantages of core–shell spectroscopic techniques is that they can probe valence orbitals—which are responsible for bond formation and are therefore delocalized over the entire molecular edifice—from atomic-like levels. The initial state of the transition is a (core) orbital that is local-

ions. So, would symmetry be conserved in this case?

To answer this question, the authors used a subtle approach.[1] Core levels decay in many cases by emission of an Auger electron, while an electron from a higher orbital fills the initially created core hole. The lifetime of the latter is

sion coincidence spectroscopy (APECS) they used, and other coincidence techniques (such as double photoemission[8]) to "condensed matter" systems (i.e. clusters, surfaces, and solids). In this context, the localization or delocalization of the core hole becomes an issue.

Most core-level spectroscopic studies

Attosecond photoionization of a coherent superposition of bound and dissociative molecular states: effect of nuclear motion

by

André D. Bandrauk,

with S.Chelkowski, G.L. Yudin,
Université de Sherbrooke, Canada

P.B. Corkum (Ottawa),
J. Manz (Berlin)

J Phys B 42,134001 (2009)

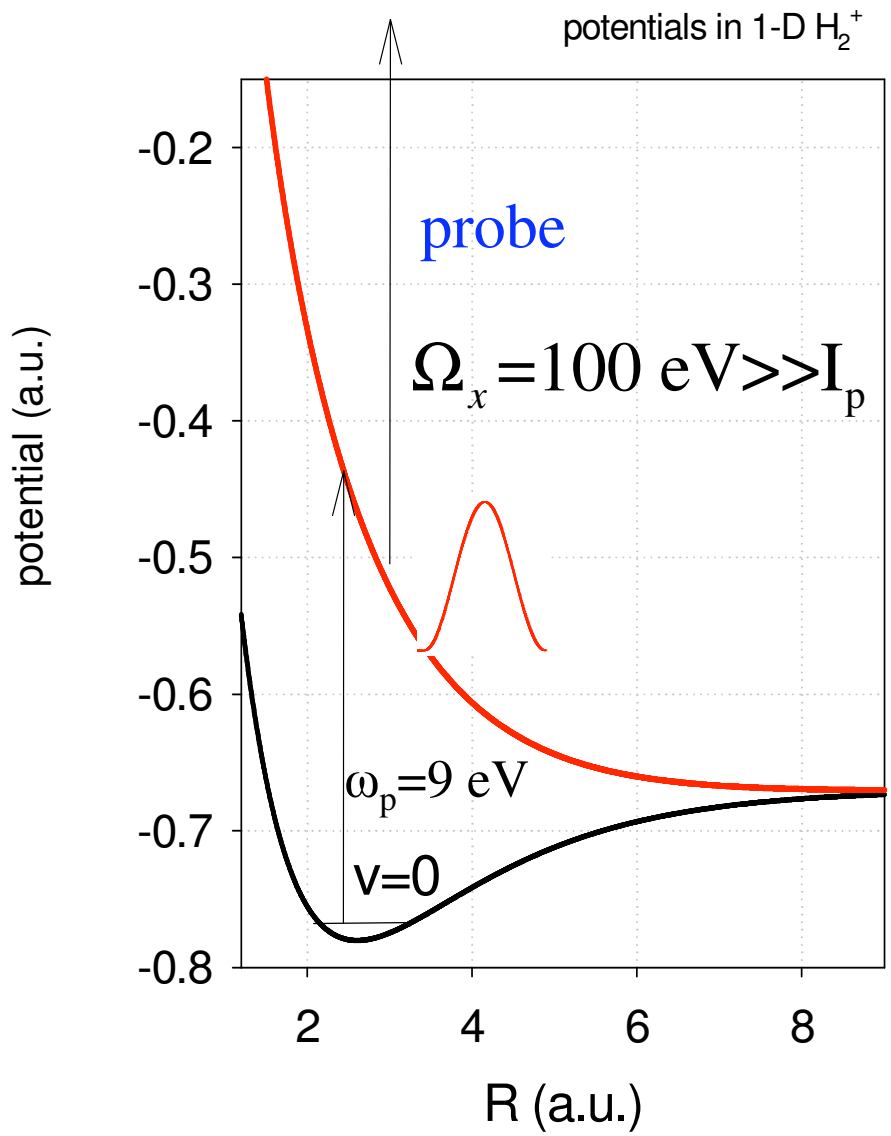

Electric field of a pump pulse E_p and of an attosecond probe E_X

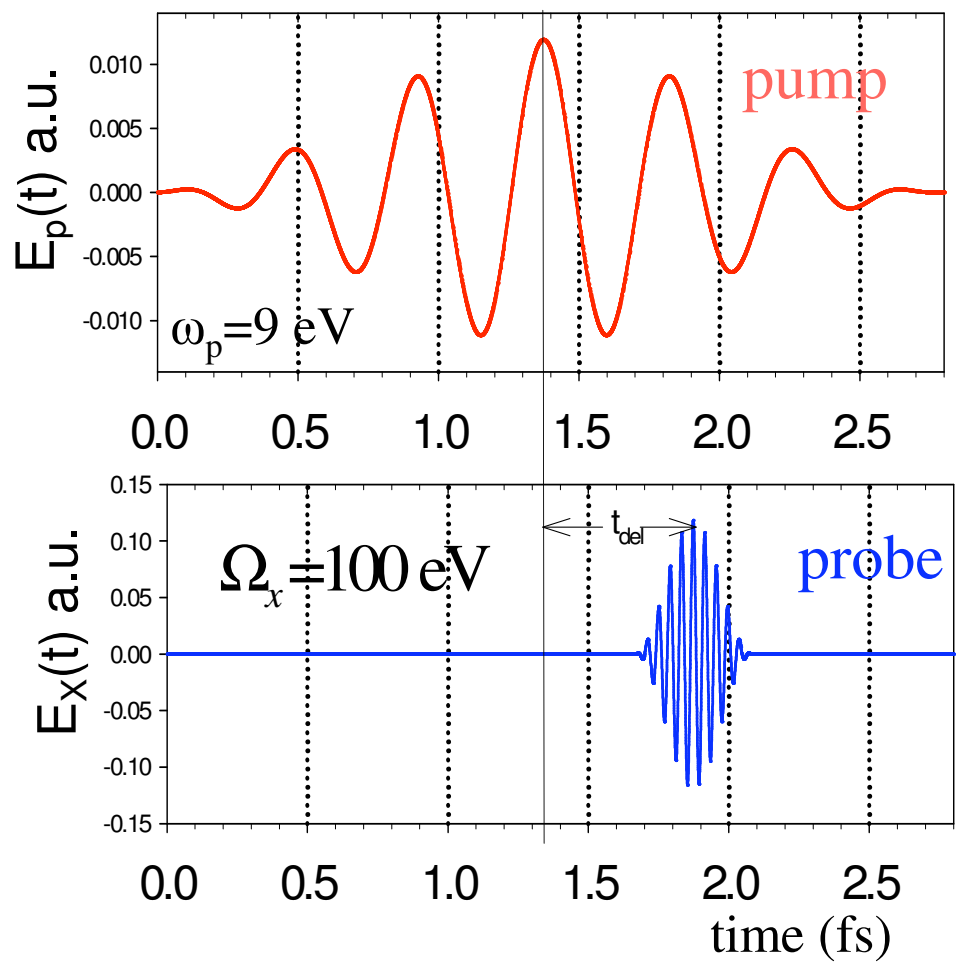

We solved the TDSE for a series of delays: t_{del}= 0.5fs + k T_1 / 8 , k=0,1,.. $T_1=2\pi/\omega_p$. We calculated the forward and backward) photoelectron spectra S(p) T1/8= 0.46 fs

PRA 57,1176(1998)

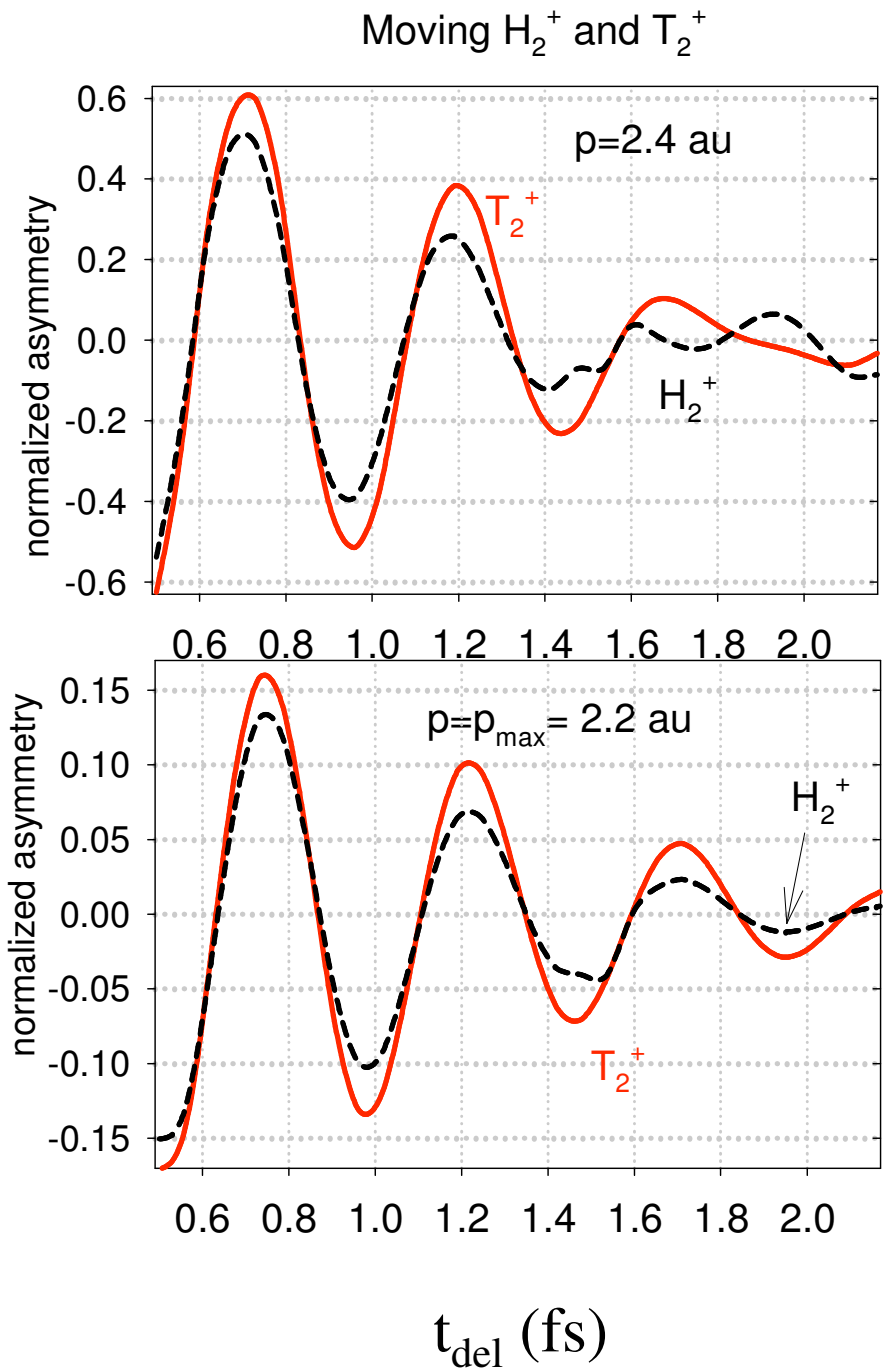

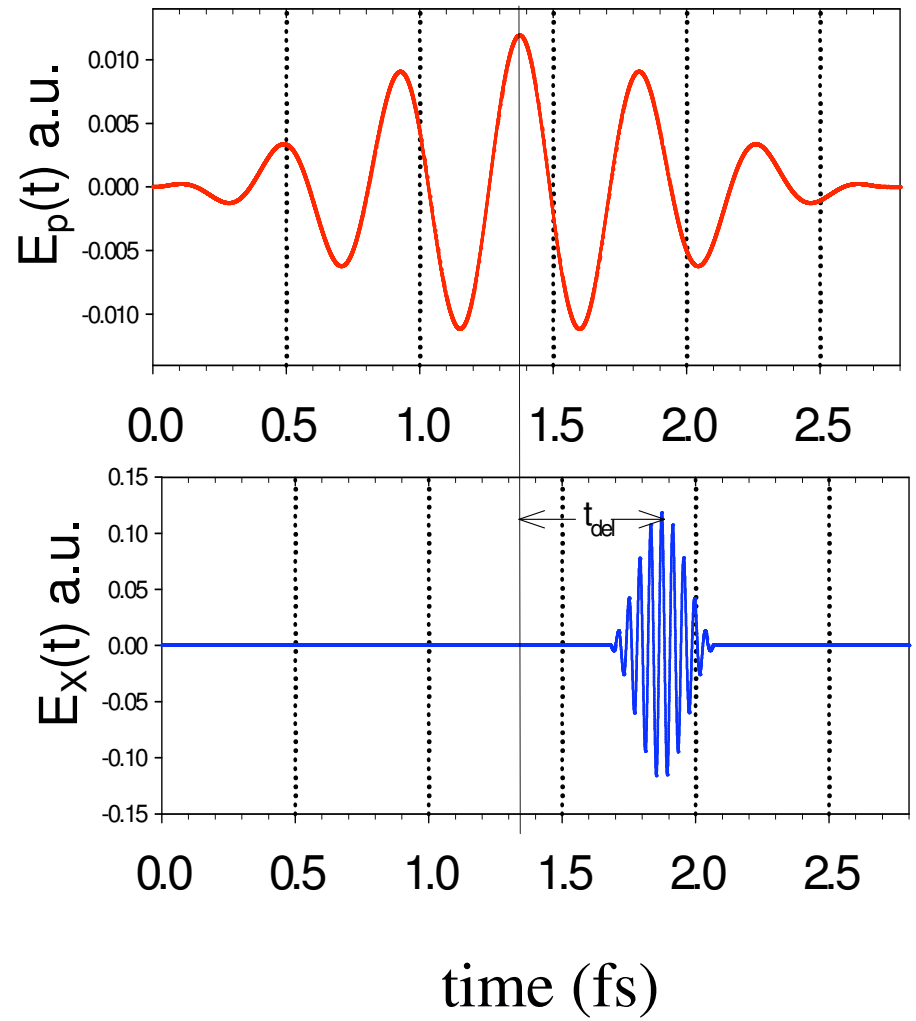

$$\text{asymmetry}=\frac{S_{\text{forw.}}(p)-S_{\text{backw.}}(p)}{S_{\text{forw.}}(p)+S_{\text{backw.}}(p)}$$

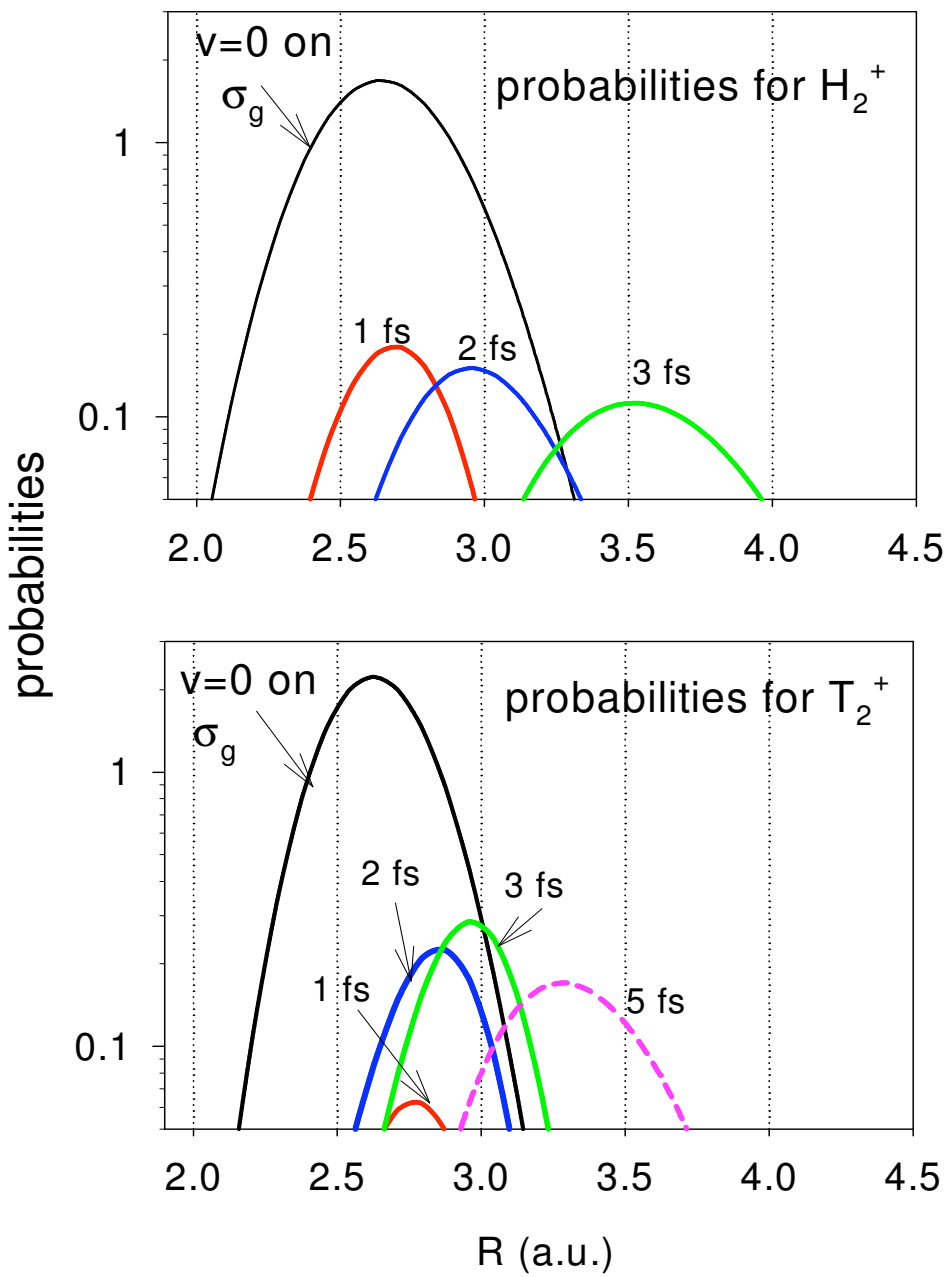

Wave packet motion induced by the pump shown below:

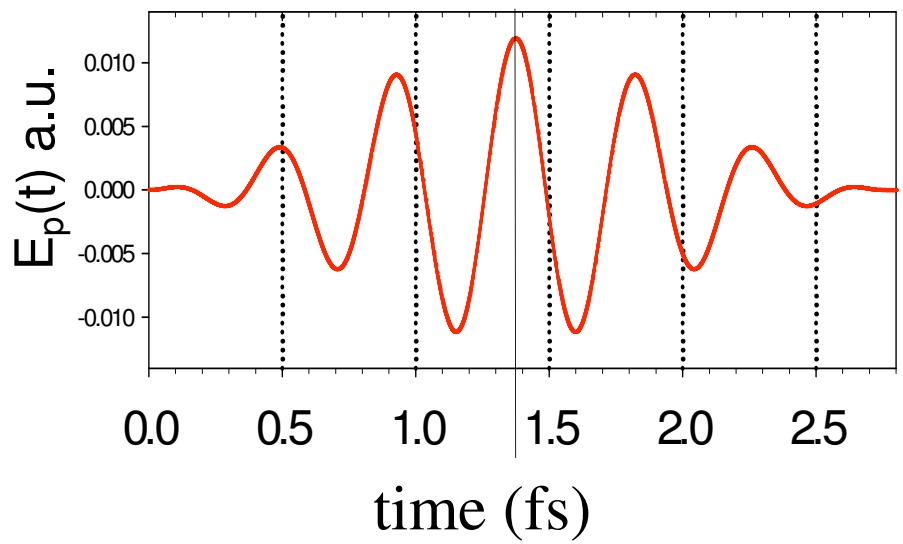

We show the initial v=0 vibrational state and the dissociating packets on σ_u.

Conclusion: at t>3 fs (t_{del} > 1.5fs we loose the overlap in H_2^+. This agrees with the attenuation seen in the previous slide

Decoherence ?: see Zurek, PRD 47,488(1993)

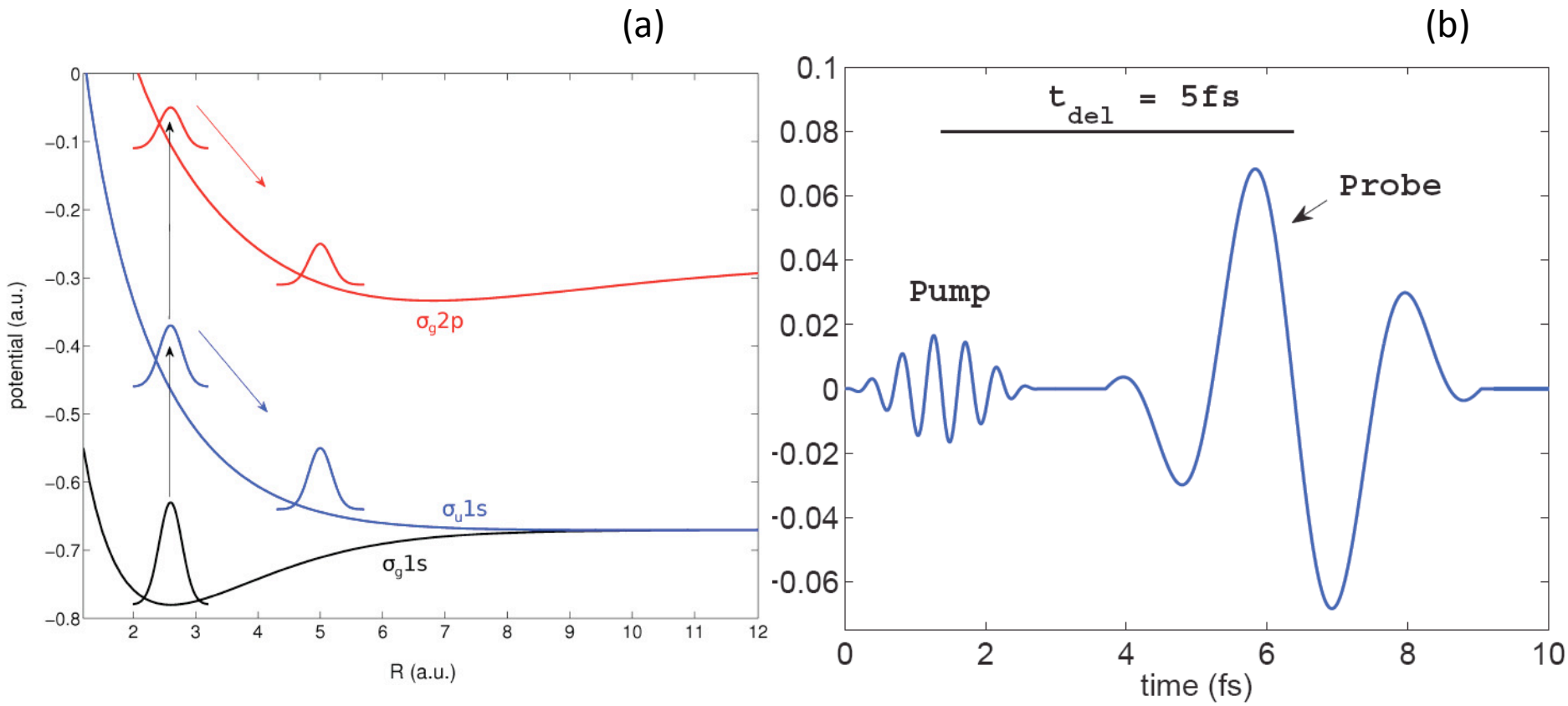

Fig.1. Illustration of the pump-probe scheme.

T Bredtmann,(FU Berlin),S Chelkowski,ADB

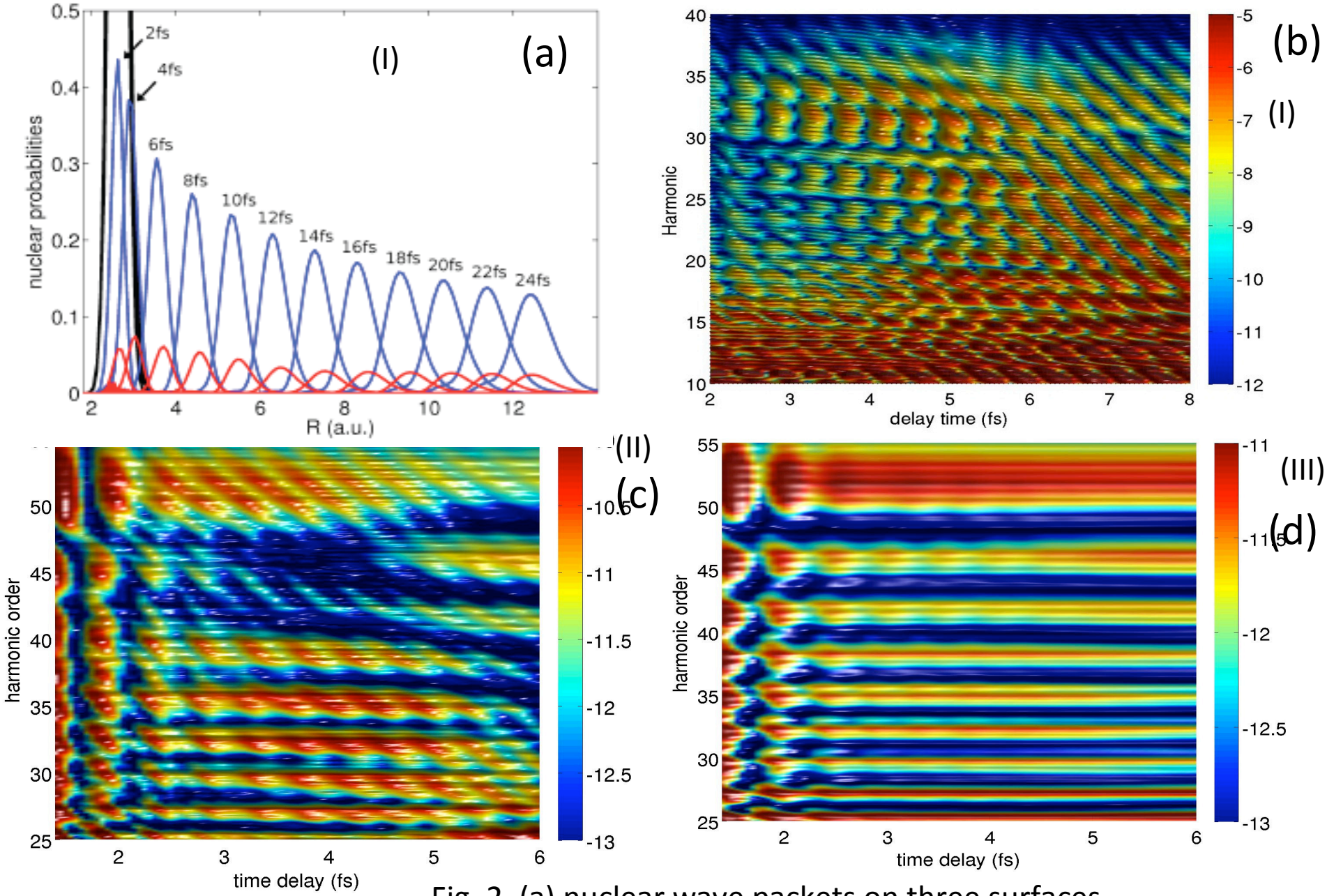

Fig. 2. (a) nuclear wave packets on three surfaces.
(b)-(c) Harmonic spectra as function of the delay time t_{del}

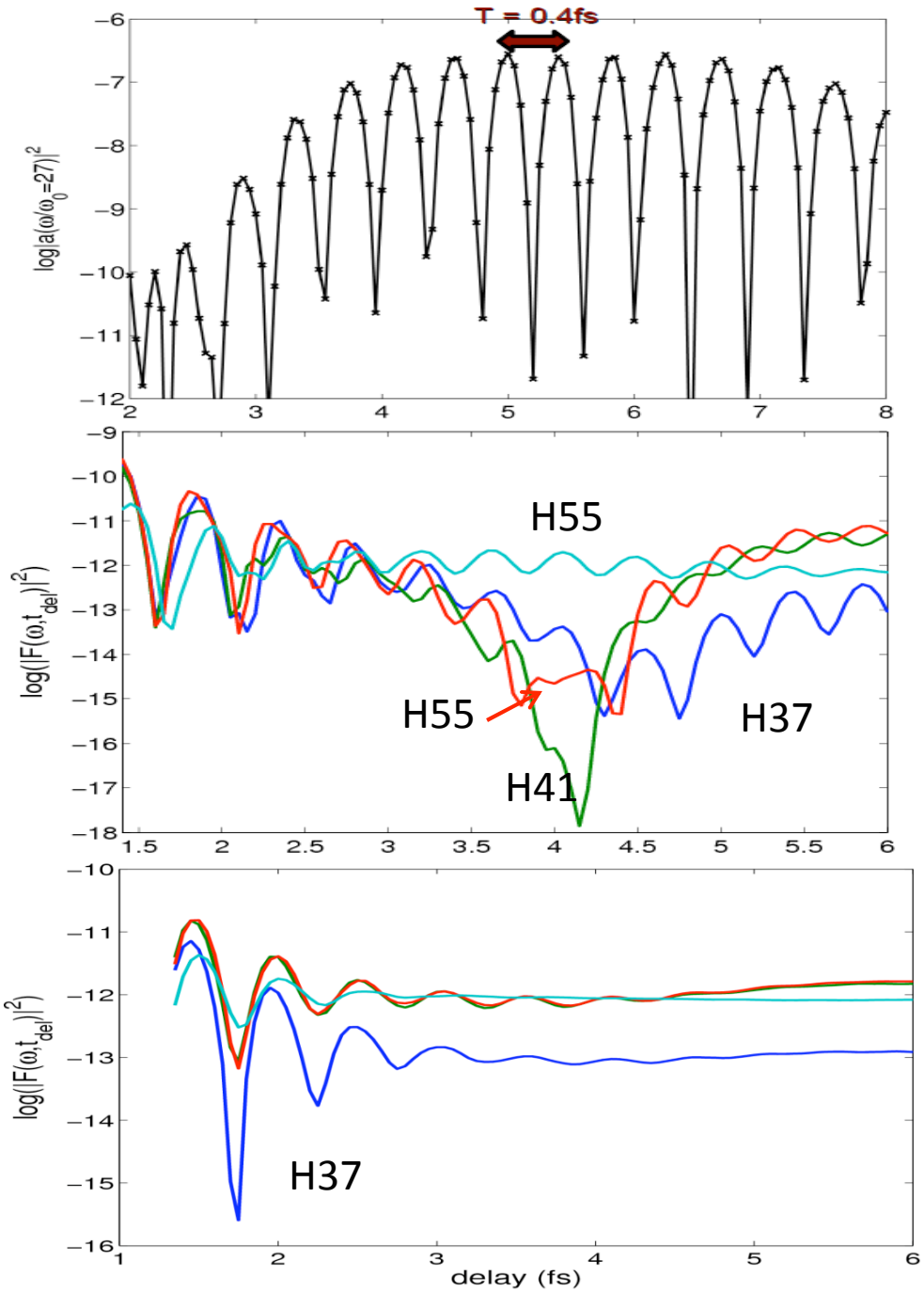

(I)

(II)

(III)

Fig.3. Intensity of selected harmonics as function of time delay t_{del} .

t_{del} = 5.0 fs (a)

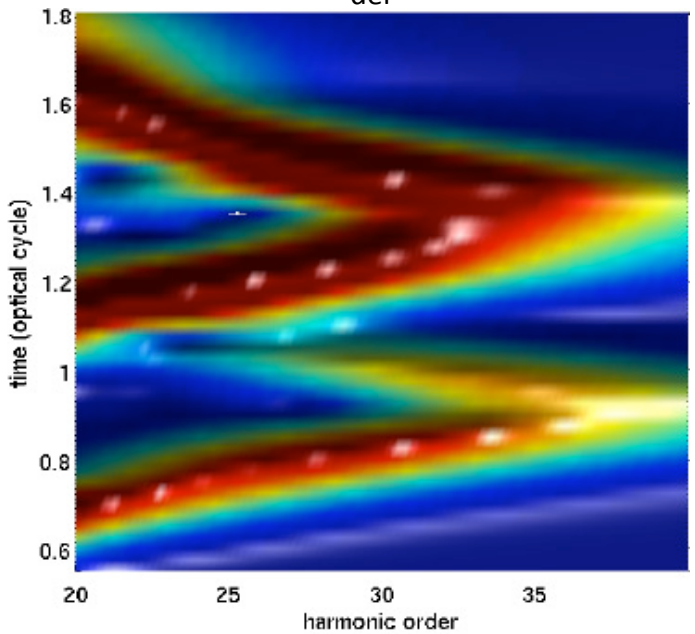

t_{del} = 5.2 fs (b)

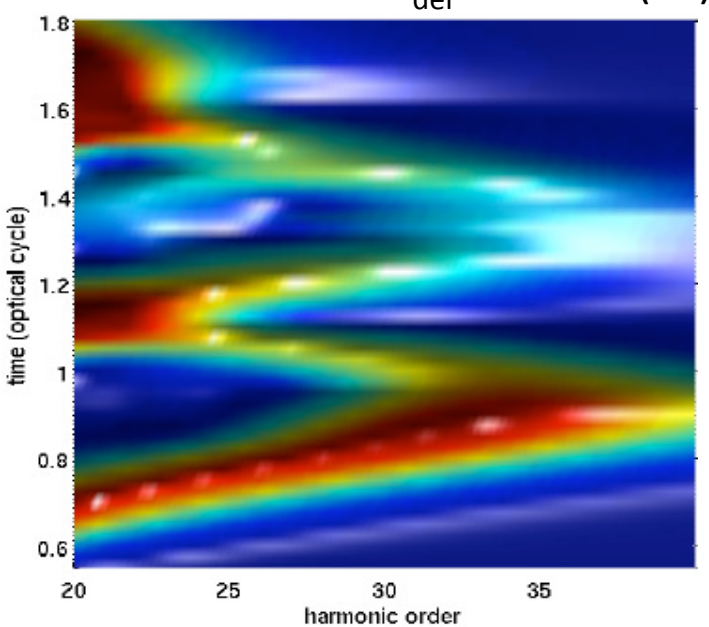

(c)

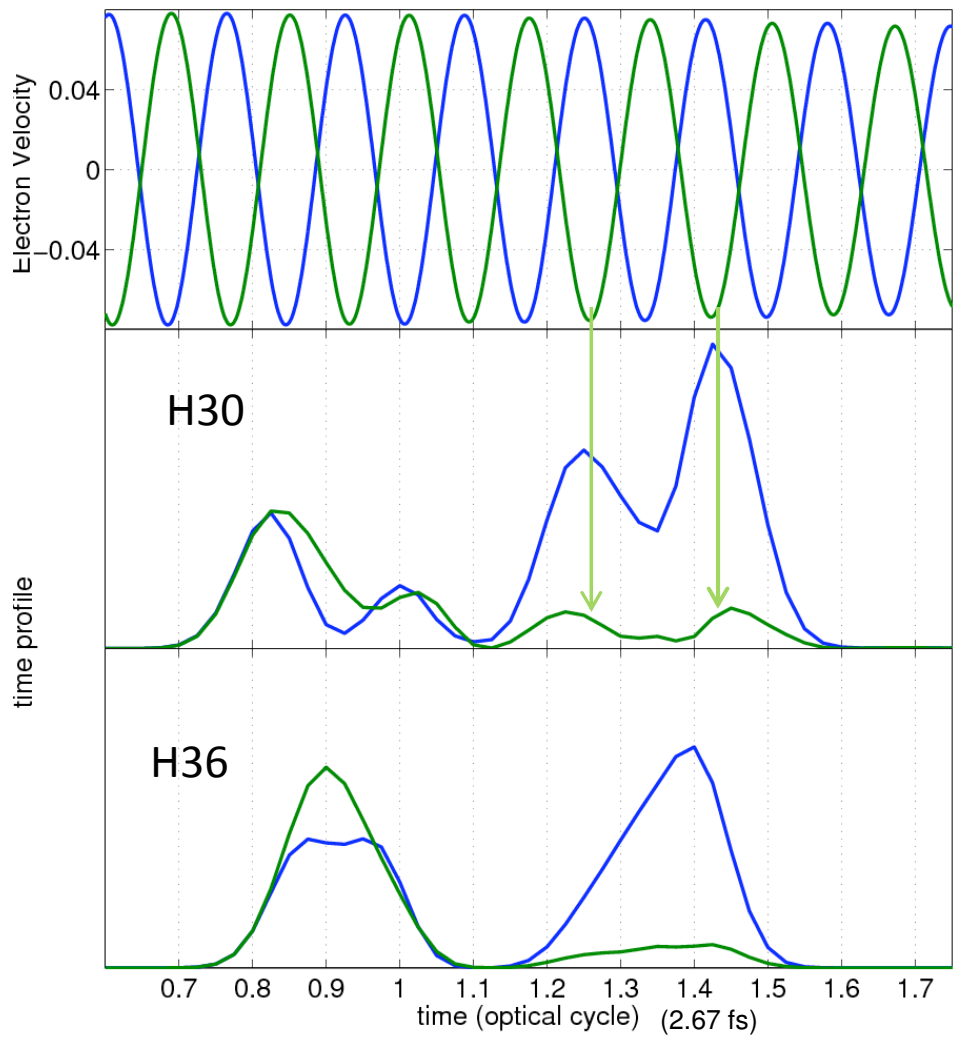

Fig.4 Time-profiles for the scheme (I) , blue - t_{del}=5.0, green- t_{del}=5.2fs

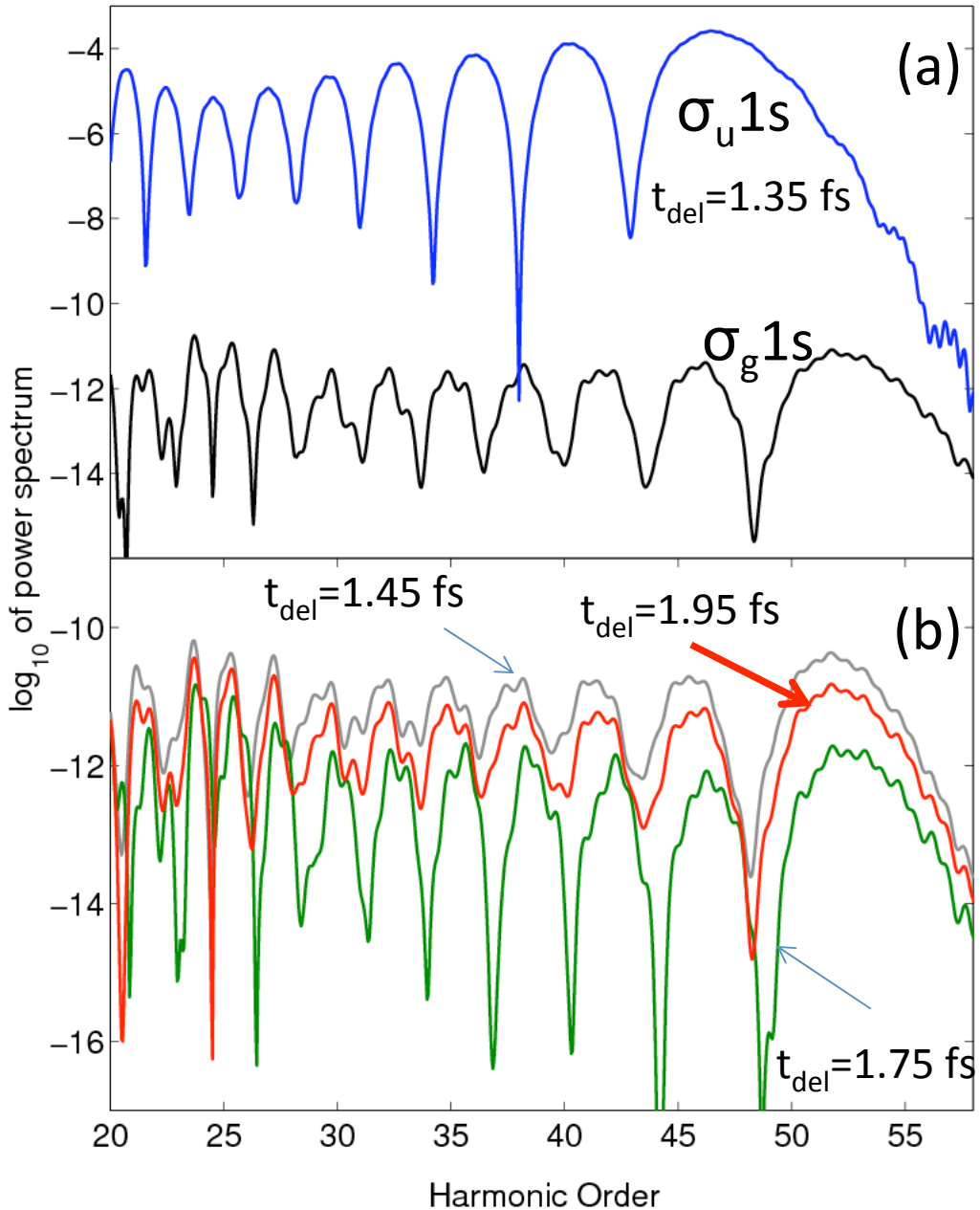

Fig.5 Harmonic spectra for $I_{probe}=4\times10^{14}W/cm^2$ generated from : (a) σ_g1s (red) and σ_u1s (blue), and from : (b) coherent superposition at delays 1.45, 1.75 and 1.95 fs (scheme III) .

Nuclear fusion from explosions of femtosecond laser-heated deuterium clusters

T. Ditmire, J. Zweiback, V. P. Yanovsky, T. E. Cowan, G. Hays & K. B. Wharton

Laser Program, L-477, Lawrence Livermore National Laboratory, Livermore, California 94550, USA

As a form of matter intermediate between molecules and bulk solids, atomic clusters have been much studied[1]. Light-induced processes in clusters can lead to photo-fragmentation[2,3] and Coulombic fission[4], producing atom and ion fragments with a few electronvolts (eV) of energy. However, recent studies of the photoionization of atomic cluster) are ionized, electrons undergo rapid collisional heating for the short time (<1 ps) before the cluster disassembles in the laser field[19]. Through various collective and nonlinear processes, the laser rapidly heats the electrons to a non-equilibrium state (with mean

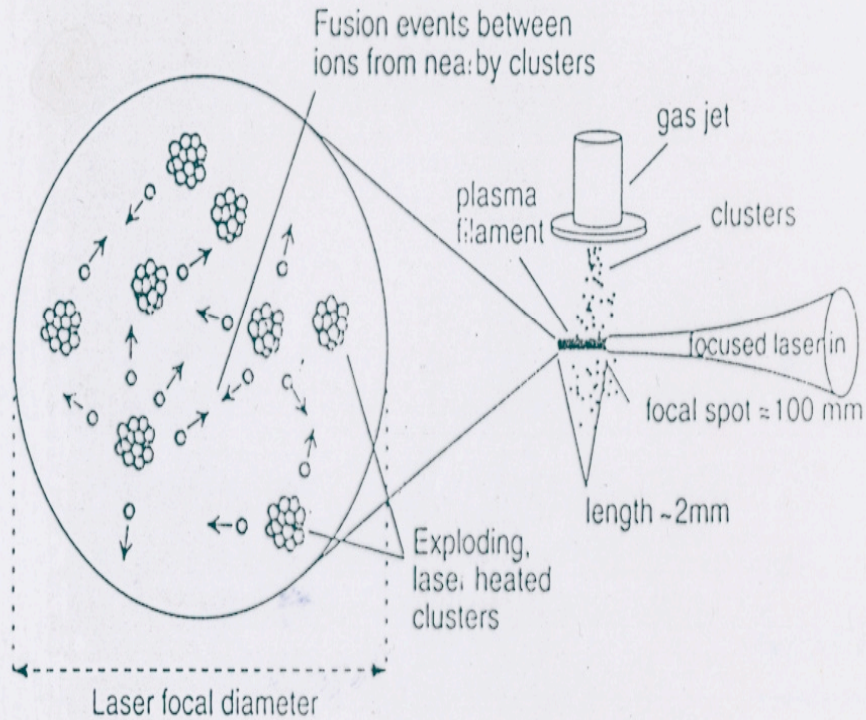

Figure 1 Layout of the deuterium cluster fusion experiment.

CREI~ Rc ~ 4 – 5 Å

RECOLLISION OF d^+ WITH A μd ATOM INITIATED BY A SUPER-INTENSE LASER

3 U_P **Recollision energy=** 1.40 MeV

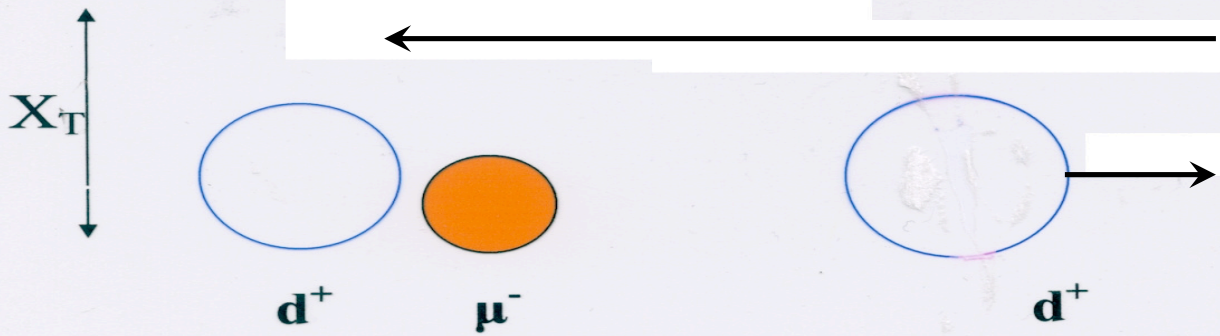

X_T =0.9 Å

ELECTRIC FIELD E(t) OF THE LASER

λ = 800 nm

THUS THE LASER CAN INITIATE

A NUCLEAR REACTION ,e.g:

I – 3 x 10^{22} W/cm^2

$$d + d \rightarrow n\ (2.45\ \text{MeV}) + {}^3He\ (0.82\ \text{Mev})$$

or

$$d + t \rightarrow n\ (14.1\ \text{MeV}) + {}^4He\ (3.5\ \text{MeV})$$

d-μ-d molecule dissociating in
200 nm, I=10^{22} W/cm^2 laser field

deuterium returns back !

E~1/2 MeV

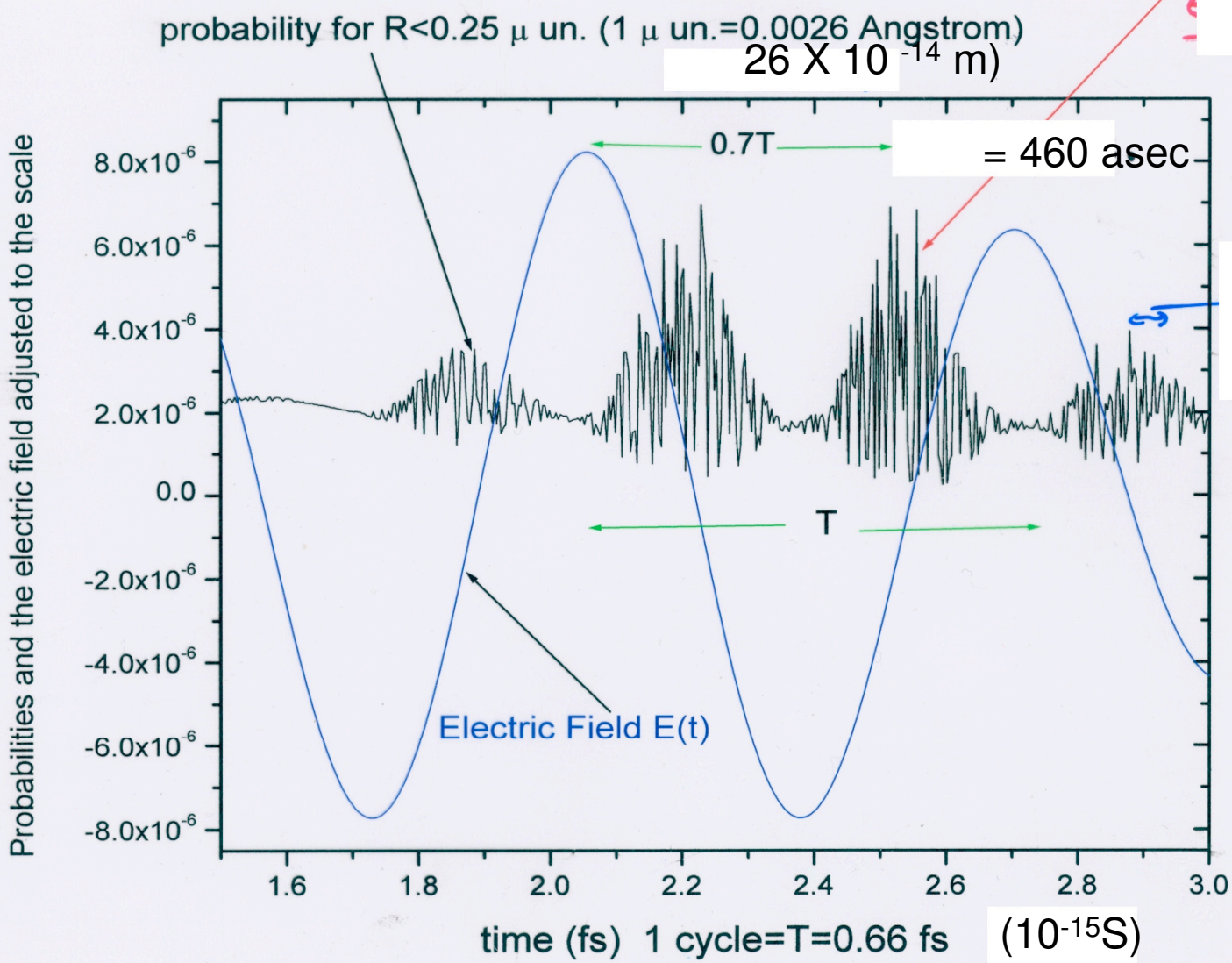

PRL 93,083602(2004) ; ADB,G Paramonov,AIP Conf Proc,1209,7(2010

Dressed Potential Energies for H_2 molecule in static laser field

e=0.106299 a.u.

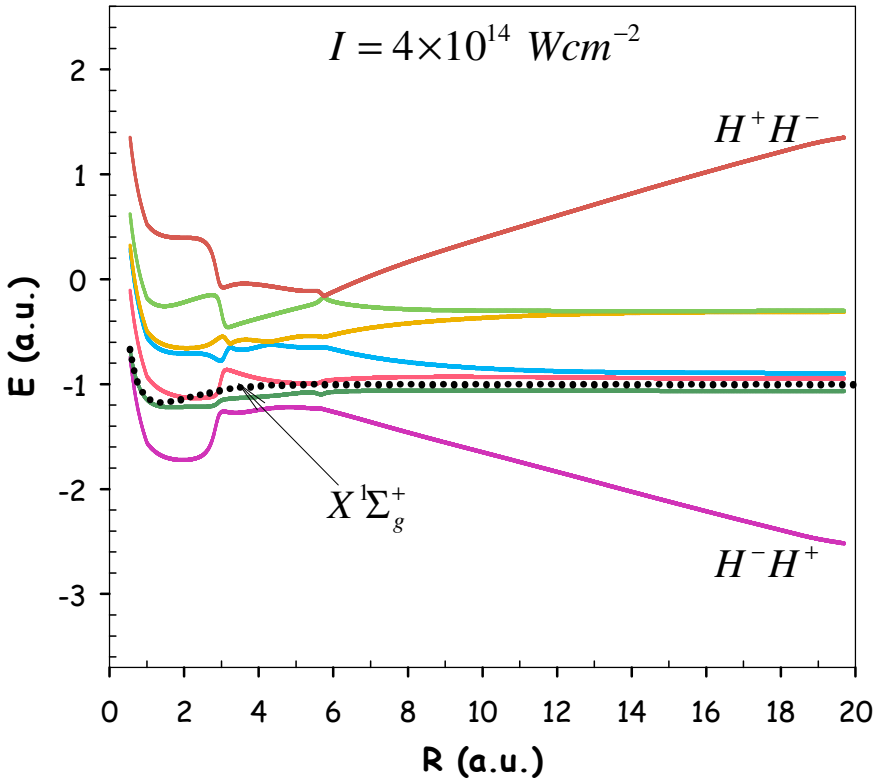

e=0.168073 a.u.

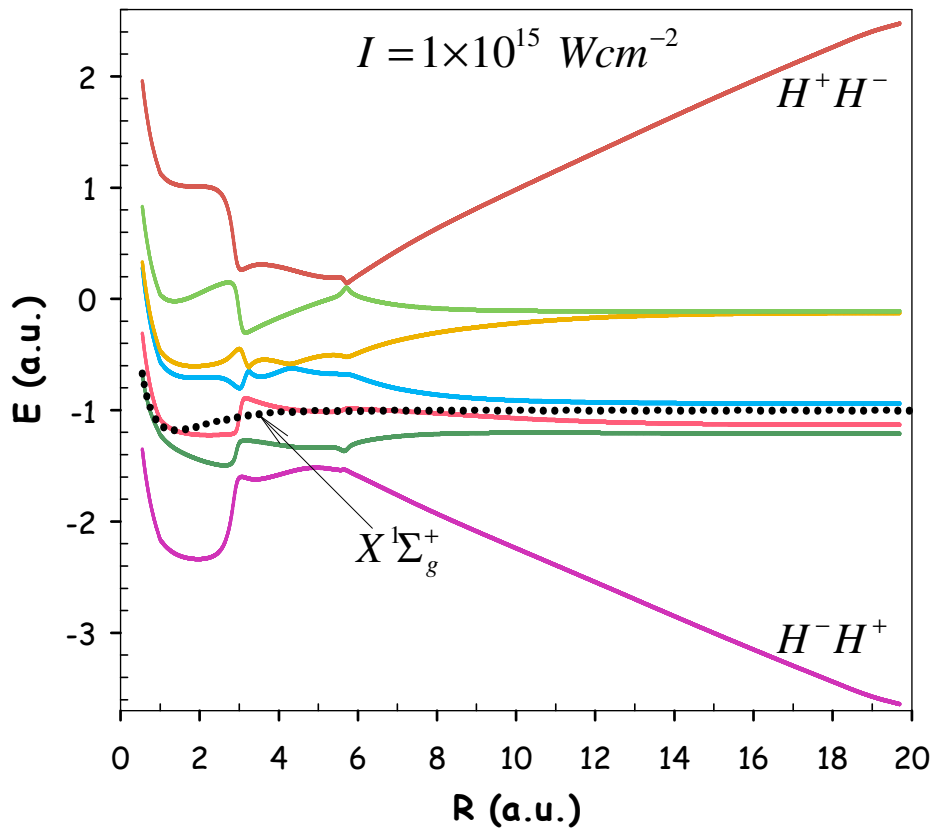

J. Phys. Chem. A 111, 9340 (2007)

APRIL 13, 2009 | VOLUME 87, NUMBER 15 | PP. 50-51
ACS MEETING NEWS

Tracking Electrons

Attosecond science opens the door to real-time observation and control of electron dynamics

Jyllian Kemsley

TEN YEARS AGO, Ahmed H. Zewail won the Nobel Prize for using femtosecond spectroscopy to study atomic motions during chemical reactions. Emerging now from Zewail's pioneering work is the ability to use femtosecond laser pulses to monitor attosecond-scale electron dynamics, which was the focus of a Divison of Physical Chemistry symposium on attosecond science at the American Chemical Society national meeting in Salt Lake City last month.

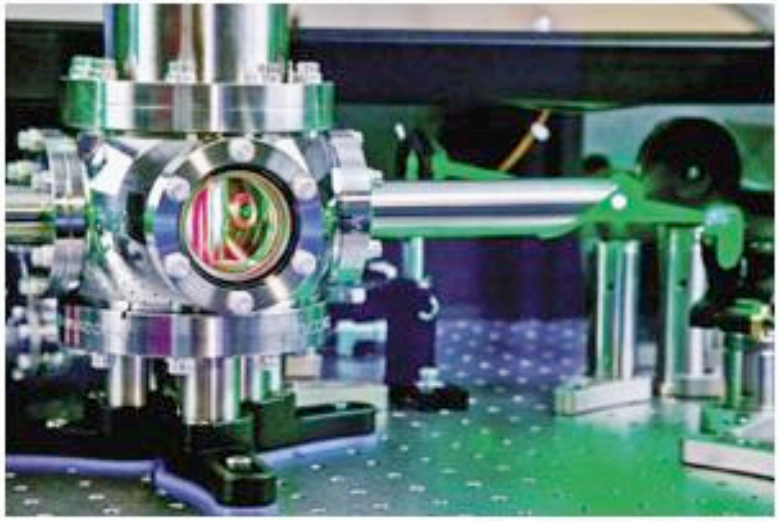

Gary Larson © 2004

ULTRAFAST A cryostat contains a cooled Ti:sapphire laser amplifier crystal that is used to generate high-power femtosecond pulses for attosecond experiments.

"There's a whole class of processes associated with electron dynamics that occur at a femtosecond timescale or less," Daniel M. Neumark, a chemistry professor at the University of California, Berkeley, said at the meeting. "These are electron dynamics processes that don't require nuclear motion. To probe them you need attosecond-scale pulses."

Mathematical Problems

1. High order SOM
2. Multiscale time frequency analysis
3. Infinite D Optimal Control theory
   (Bartels,Murnane,Rabitz,PRA 70,043404(2004) ;ADB et al,PRA 69,041802(2004))
4. High order NLSE
5. Relativistic QM
6. Molecular movies
   (Dynamic Imaging of Electrons-Nuclei)

Springer
the language of science

springer.com

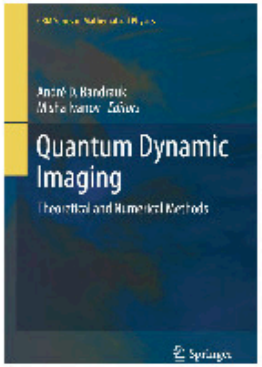

233 pages
79 illus., 76 in color
Hardcover
ISBN 978-1-4419-9490-5
$129.00

Forthcoming
May 2011

CRM Series in
Mathematical Physics

CENTRE
DE RECHERCHES
MATHÉMATIQUES

Quantum Dynamic Imaging

Theoretical and Numerical Methods

Editors:
André D. Bandrauk, Université de Sherbrooke, QC, Canada
Misha Ivanov, Imperial College London, UK

Studying and using light or "photons" to image and then to control and transmit molecular information is among the most challenging and significant research fields to emerge in recent years. One of the fastest growing areas involves research in the temporal imaging of quantum phenomena, ranging from molecular dynamics in the femto (10^{-15}s) time regime for atomic motion to the atto (10^{-18}s) time scale of electron motion. In fact, the attosecond "revolution" is now recognized as one of the most important recent breakthroughs and innovations in the science of the 21st century. A major participant in the development of ultrafast femto and attosecond temporal imaging of molecular quantum phenomena has been theory and numerical simulation of the nonlinear, non-perturbative response of atoms and molecules to ultrashort laser pulses. Therefore, imaging quantum dynamics is a new frontier of science requiring advanced mathematical approaches for analyzing and solving spatial and temporal multidimensional partial differential equations such as Time-Dependent Schroedinger Equations (TDSE) and Time-Dependent Dirac equations (TDDEs for relativistic phenomena). These equations are also coupled to the photons in Maxwell's equations for collective propagation effects. Inversion of the experimental imaging data of quantum dynamics presents new mathematical challenges in the imaging of quantum wave coherences on subatomic (subnanometer) spatial dimensions and multiple timescales from atto to femto and even nanoseconds.

In ***Quantum Dynamic Imaging: Theoretical and Numerical Methods***, leading researchers discuss these exciting state-of-the-art developments and their implications for R&D in view of the promise of quantum dynamic imaging science as the essential tool for controlling matter at the molecular level.

Key Features:

- Presents the latest research results in ultrafast imaging of quantum phenomena
- Demonstrates the wide-ranging potential of quantum dynamic imaging for R&D in areas as diverse as optoelectronics, materials science, and quantum information
- Edited and written by international leaders in the field

➢ **Table of Contents and Order Form on Reverse**

High-Energy QED: Real and Virtual Pairs

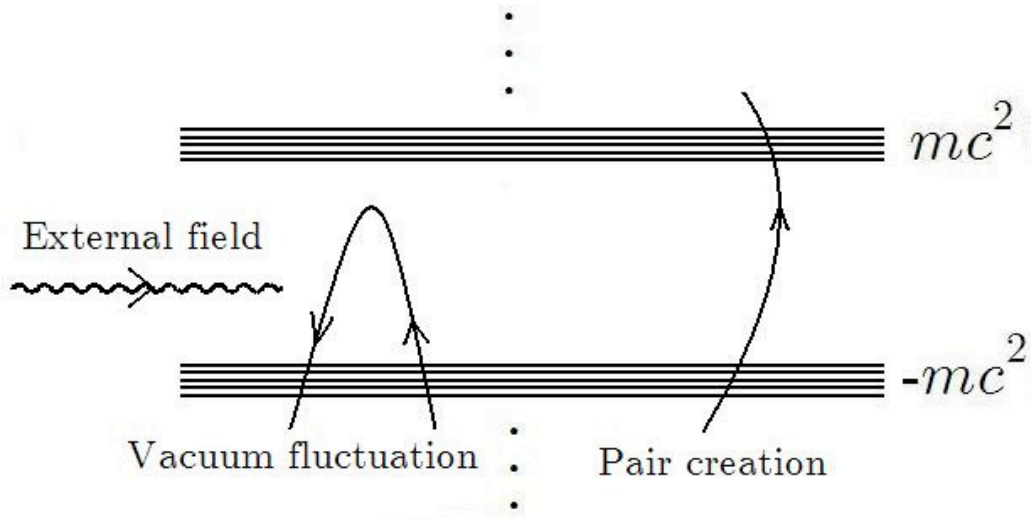

Courtesy of

CH Keitel(MPI,hdb)

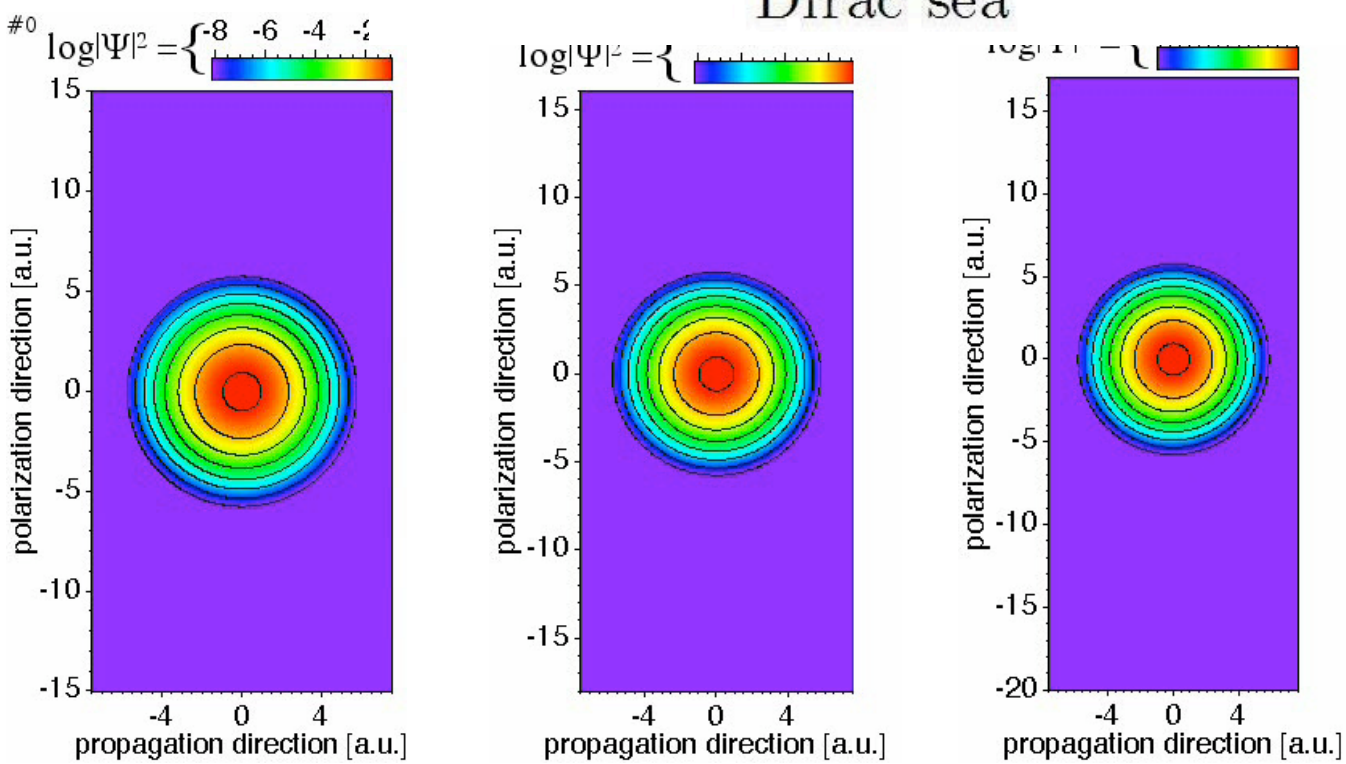

Dirac dynamics of an electron with negative energy in crossed laser beams: pairs from 10^{26} W/cm^2

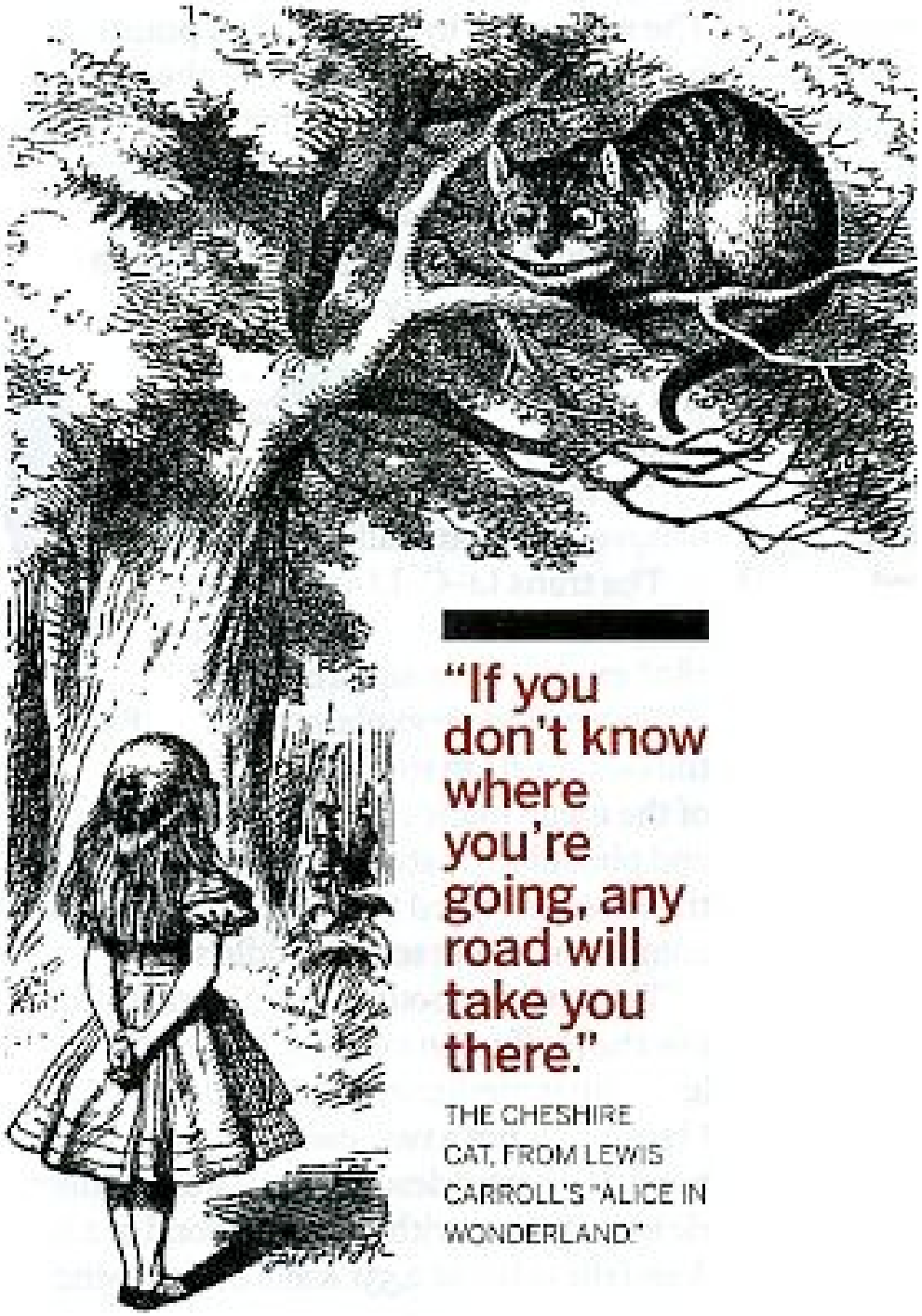

"If you don't know where you're going, any road will take you there."

THE CHESHIRE CAT, FROM LEWIS CARROLL'S "ALICE IN WONDERLAND."

International Journal of Quantum Chemistry

Volume 38 Issue 2, Pages 191 - 208

Published Online: 19 Oct 2004

Article

Theoretical approach to reactions of polyatomic molecules

L. Zülicke, A. Merkel

Akademie der Wissenschaften der DDR, Zentralinstitut für physikalische Chemie, DDR-1199 Berlin, German Democratic Republic

ABSTRACT

A scheme for systematic reduction of the theoretical treatment of elementary reactions involving polyatomic molecules is described; it consists of (1) limitation to the energetically relevant regions of the nuclear configuration space (the reaction path and its near environs) and (2) restriction to the dynamically relevant subspace of the nuclear configuration space (the active modes). Starting from a generalized reaction path Hamiltonian of Nauts and Chapuisat allowing for the use of arbitrary curvilinear coordinates and several large-amplitude modes, the realization of the above-sketched scheme is discussed. A compilation of recent work along these lines, mostly based on the simplified Miller-Handy-Adams reaction path Hamiltonian, is given with particular emphasis on applications of a statistical adiabatic model.

Received: 14 February 1989; Accepted: 4 July 1989

DIGITAL OBJECT IDENTIFIER (DOI)

10.1002/qua.560380214 About DOI

Association francophone pour le savoir – Acfas

209 - Science Laser Ultrarapide-Femto-Atto-Zeptoseconde-FAZS

Responsables

Andre BANDRAUK, Université de Sherbrooke
François LÉGARÉ, INRS

Informations sur le colloque

Catégorie : Colloque

Description du colloque :
La science laser moderne a subit une révolution par la génération d'impulsion ultracourte (quelques cycles optiques) et intense (>10^15 W/cm^2). Ceci permet l'étude de l'interaction laser-matière dans un nouveau régime hautement nonlinéaire et non-perturbatif. Le Québec est très actif et dominant dans ce domaine grâce à des laboratoires comme ALLS (Advanced Laser Light Source) situé à l'INRS-EMT, le Centre d'Optique, Photonique et Laser (COPL) de l'Université Laval, et l'équipe Atto-Québec financé par le FQRNT, etc. Un réseau de calcul de haute performance, RQHP, membre de Calcul Canada permet d'exécuter des simulations de haut niveau pour guider les expérimentateurs. Ce colloque propose donc de rassembler les acteurs principaux du Quebec en plus quelques sommités internationales (françaises) pour adresser les questions importantes d'applications futures à de nouvelles technologies importantes pour la société de l'avenir.

Sessions

Lundi 9 mai 2011

Science Laser Ultrarapide-Femto-Atto-Zeptoseconde-FAZS

08:25 - 12:00
UdeS- Éducation-A2-021
Type : orale

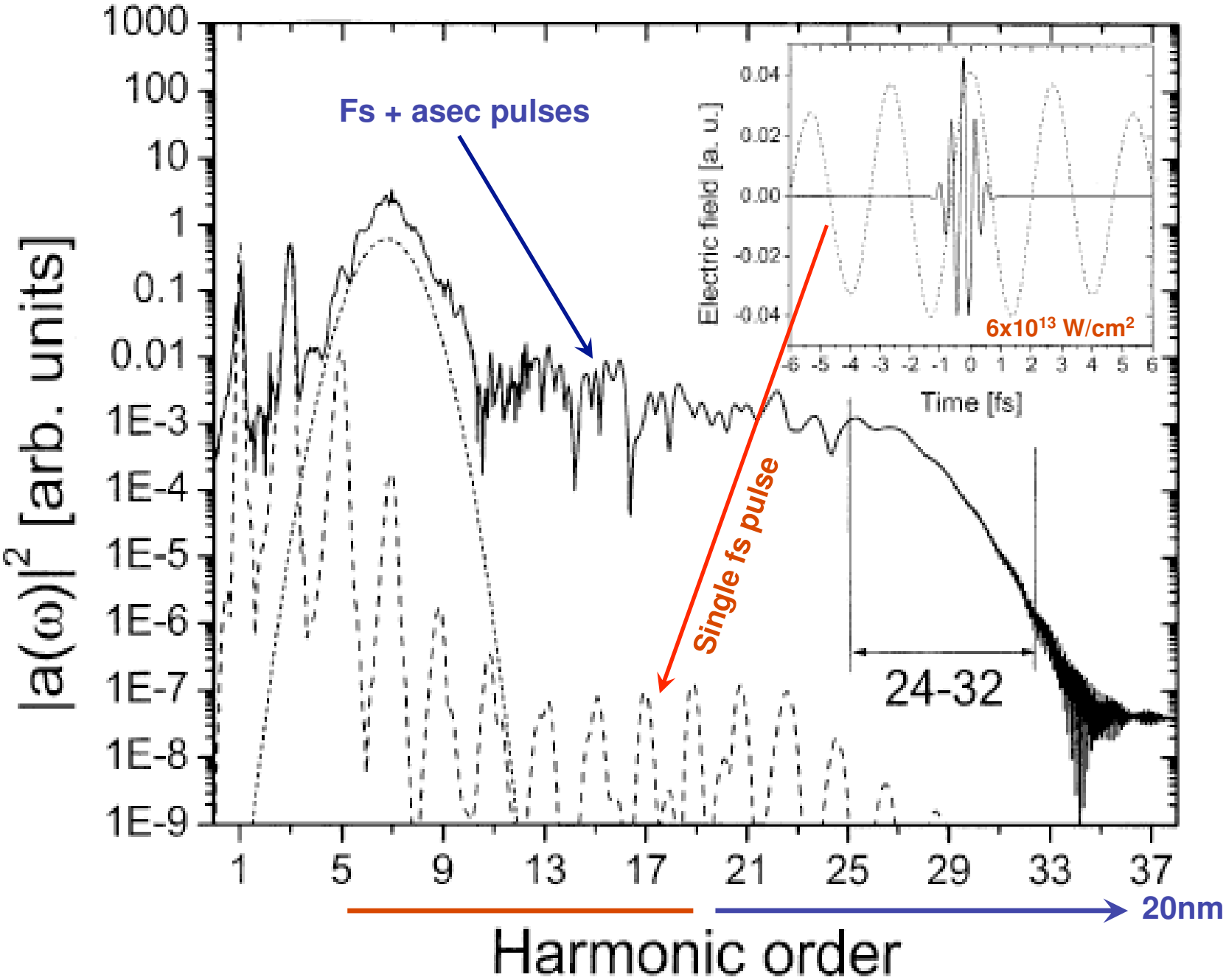
Fs + asec pulses
Single fs pulse
24-32
6x10^13 W/cm^2
Electric field [a. u.]
Time [fs]
|a(ω)|^2 [arb. units]
Harmonic order
20nm

RÉSEAU QUÉBÉCOIS
DE CALCUL DE HAUTE PERFORMANCE

Rapport annuel 2008

1er janvier au 31 décembre

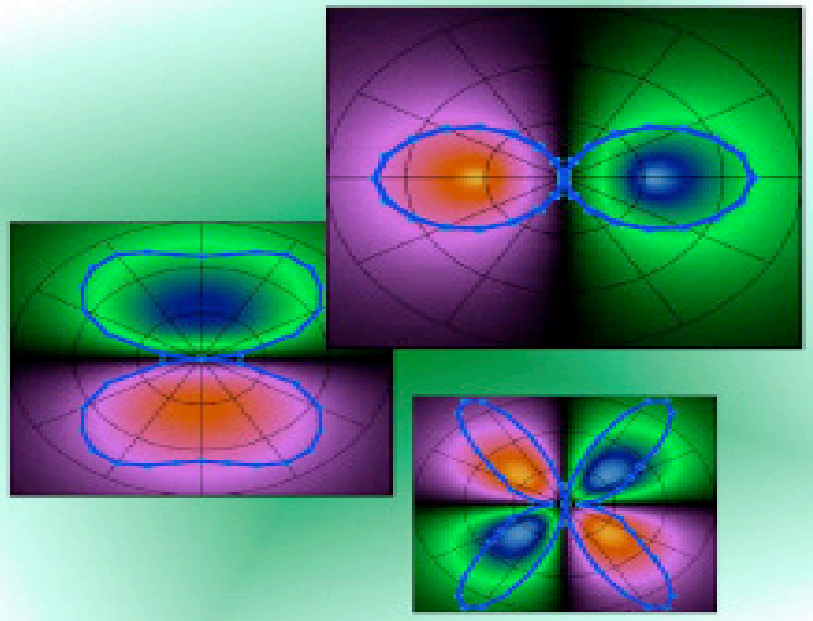

PRA Kaleidoscope Images: October 2009

Many Physical Review articles contain images that not only convey important scientific information, but also are visually pleasing. The editors showcase a selection of images from published articles (read the announcement). The selections are based on aesthetics, not on the scientific merit of the paper. The figures may be slightly modified from the published version. Recently published images also appear on our main page.

Click on each thumbnail to see the full image and link to the paper.